Towards A Tri-View Diffusion Framework for Recommendation

Ximing Chen University of Macau Macau SAR, China yc37921@um.edu.mo Pui Ieng Lei University of Macau Macau SAR, China yc37460@um.edu.mo Yijun Sheng University of Macau Macau SAR, China yc17419@um.edu.mo

Yanyan Liu University of Macau Macau SAR, China yc07402@um.edu.mo Zhiguo Gong* University of Macau Macau SAR, China fstzgg@um.edu.mo

Abstract

Diffusion models (DMs) have recently gained significant interest for their exceptional potential in recommendation tasks. This stems primarily from their prominent capability in distilling, modeling, and generating comprehensive user preferences. However, previous work fails to examine DMs in recommendation tasks through a rigorous lens. In this paper, we first experimentally investigate the completeness of recommender models from a thermodynamic view. We reveal that existing DM-based recommender models operate by maximizing the energy, while classic recommender models operate by reducing the entropy. Based on this finding, we propose a minimalistic diffusion framework that incorporates both factors via the maximization of Helmholtz free energy. Meanwhile, to foster the optimization, our reverse process is armed with a well-designed denoiser to maintain the inherent anisotropy, which measures the user-item cross-correlation in the context of bipartite graphs. Finally, we adopt an Acceptance-Rejection Gumbel Sampling Process (AR-GSP) to prioritize the far-outnumbered unobserved interactions for model robustness. AR-GSP integrates an acceptancerejection sampling to ensure high-quality hard negative samples for general recommendation tasks, and a timestep-dependent Gumbel Softmax to handle an adaptive sampling strategy for diffusion models. Theoretical analyses and extensive experiments demonstrate that our proposed framework has distinct superiority over baselines in terms of accuracy and efficiency.

CCS Concepts

 $\bullet \ Information \ systems \rightarrow Recommender \ systems.$

Keywords

recommender systems, diffusion models, hard negative samplings

ACM Reference Format:

Ximing Chen, Pui Ieng Lei, Yijun Sheng, Yanyan Liu, and Zhiguo Gong. 2025. Towards A Tri-View Diffusion Framework for Recommendation. In Proceedings of 32nd ACM SIGKDD Conference on Knowledge Discovery and

*Corresponding author.



This work is licensed under a Creative Commons Attribution International 4.0 License.

KDD '26, Jeju, Korea

© 2025 Copyright held by the owner/author(s). Publication rights licensed to ACM. ACM ISBN 978-1-4503-XXXX-X/2018/06 https://doi.org/XXXXXXXXXXXXXXX Data Mining (KDD '26). ACM, New York, NY, USA, 13 pages. https://doi.org/XXXXXXXXXXXXXXX

1 Introduction

Recommendation systems persist as an escalating and influential research field in response to information overload, yet confront mounting challenges, such as data sparsity and diversity. Over these years, diffusion models (DMs) [18, 19, 35] have established themselves as powerful tools in recommendations tasks [5, 54, 55], demonstrating remarkable capability in noise smoothing, dimensionality reduction, and prediction generation. Various diffusion-based recommender approaches [36] - including social recommendation [30, 33], sequential recommendation [38, 63], and cross-domain recommendation [32, 68] - have achieved notable prominence. Despite their success, existing diffusion-based recommenders have not rigorously examined DMs in recommendation tasks.

A primary focus of existing DM-based recommender models is their reliance on the denoising and regenerating mechanism in the reverse process. Intuitively, researchers presume that iteratively refining noisy user-item interactions through a gradual denoising process can capture nuanced user preferences more effectively than deterministic and single-step generative approaches, in spite of any loss used for training convergence [20]. However, the latest work [38] has argued that existing DM-based recommender models blindly adopt original objectives (e.g., Mean Squared Error (MSE)) from other fields [18, 48], without examining them from the perspective of recommendation tasks. As shown in Figure 1, classic recommendation objectives (e.g., Bayesian Personalized Ranking (BPR) [42]) consider the essential role of negative items, which enhances personalization performance by maximizing the decision boundary P(Item|User). On the other hand, MSE is intrinsically capable of mitigating data sparsity with the joint distribution P(Item, User) [34], whereas its potential in ranking implicit feedback is suboptimal [4]. Although a surrogate optimization target is proposed for sequential recommendations based on BPR and MSE, its elusive design leads to biphasic oscillation [16] due to the intertwined learnable parameters in the denoiser during training, and fails to converge in general recommendation tasks eventually. Hence, it naturally gives rise to the question: How to elucidate and utilize the characteristic of losses with concision and profundity?

To investigate this issue, we first conduct pilot experiments on two genres of models: DiffRec [55] for DM-based recommender models, while BPR [42] and LightGCN [14] for the classic ones. Two

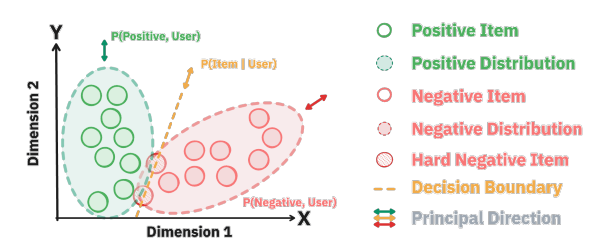


Figure 1: Toy illustration of 2D visualization on items.

metrics are of consideration: energy [12] demonstrates the number of reconstructed interactions after training, while entropy [44] qualifies the uncertainty of reconstructed items' distribution. The visualization shows that during optimization, DiffRec maximizes an energy function, while BPR and LightGCN minimize entropy. Therefore, from the thermodynamic view, follow-up questions come up: (1) How to judiciously design training objectives for two genres in general? and (2) How to organize them effectively and efficiently?

For the first question, a minimalist diffusion framework that incorporates both genres of objectives via *Helmholtz free energy* [72] is spontaneously proposed. It follows the concept from thermodynamics based on our observations from pilot experiments. However, the limitation of DM-based models in capturing high-order collaborative signals [5, 66, 71] hinders an effective integration of both objectives for the second question. Specifically, the inherent anisotropy of user-item interactions, which manifests the topological information (i.e., principal direction [9] in Figure 1) embedded in the hyperbolic space [49], is impaired by adding progressive isotropic Gaussian noise. Thus, the results might underperform either genre of models as the undertrained decision boundary deteriorates the joint-training of both genres of objectives mutually.

The demand for robustness of the mutual joint-training objective also necessitates an efficient yet effective negative sampling method. This approach must adequately refine the decision boundary along with the item distribution. However, classic recommender models typically rely on random negative sampling (RNS) [42], which often yields uninformative negatives. Hard negative sampling (Hard NS) [39, 62] offers an improvement by focusing on samples near the decision boundary (cf. Figure 1). Yet, it compromises models' ability amid optimization and generalization via a sub-linear correlation with the positive distribution. More critically, the varying magnitude of noise across different timesteps complicates a productive sampling process for diffusion models [50].

To address these issues, we propose **TV-Diff**, a novel diffusion recommendation framework from a rigorous tri-view lens. TV-Diff employs three mutually interacting components: **Helmholtz Free Energy Maximization** incorporates designated *energy-based* and *entropy-based* training objectives to optimize the model from a thermodynamic view as a foundation of our proposed framework. **Anisotropic Denoiser** maintains the anisotropic signals by disentangling the monolithic user-wise encoder-decoder paradigm into users and items aspects, and reconstructing interactions by user-item cross-correlation measurements with explicit topological information. **Acceptance-Rejection Gumbel Sampling Process** first discards true negatives on the general aspect via an acceptance probability. Then, a timestep-dependent Gumbel Softmax is introduced to buffer the risk of mistaking true positives due to

excessive noise in the diffusion process. Rationale analyses of the last two components are also provided in the context of *Helmholtz free energy*. To summarize, key contributions of TV-Diff are:

- We present TV-Diff, a minimalistic diffusion recommender framework, to revisit diffusion models from a thermodynamic view, a topological view, and a hard-negative view. Three components are proposed to interplay and assist with each other.
- We experimentally and theoretically analyze the completeness of existing recommender models, the equivalence of BPR and *entropy* on optimization, the mechanism of topological information, and the bounds of the hard negative sampling approach.
- Extensive experiments demonstrate our diffusion framework's superiority, in terms of its performance, efficiency, and compatibility with diverse scenarios.

2 Preliminaries

Recommendation Task. Given the data of user-item interaction $\mathcal{D} = \{u, i, r_{u,i} | u \in \mathcal{U}, i \in I\}, \mathcal{U} = \{u_1, \dots, u_m\}$ denotes the user set $(|\mathcal{U}| = m), I = \{i_1, \dots, i_n\}$ denotes the item set (|I| = n), and $r_{u,i} = \{0,1\}$ indicates whether user u has interacted with item i as implicit feedback. N(u) is the interactive item set of user u. In matrix, the bipartite graph can be represented by $\mathbf{R} \in \{0,1\}^{m \times n}$. In our work, we focus on user-based Top-K recommendations, where K is the number of predicted items. We use **BOLD UPPERCASE** and **lowercase** letters to denote matrices and vectors, respectively. Diffusion Model. For a given data point $\mathbf{x}_0 \in \mathbb{R}^n$ that represents a complete interaction record of a user (a.k.a. r_u), the diffusion model [55] establishes a predefined variational distribution for the forward trajectory $q(\mathbf{x}_t | \mathbf{x}_0)$ as:

$$q(\mathbf{x}_{t}|\mathbf{x}_{0}) = \mathcal{N}(\mathbf{x}_{t}; \prod_{t'=1}^{t} \sqrt{(1-\beta_{t'})}\mathbf{x}_{0}, (1-\prod_{t'=1}^{t} (1-\beta_{t'})\mathbf{I}), \quad (1)$$

which is indexed by timesteps $t \in \{1, ..., T\}$. $\beta_t \in (0, 1)$ denotes the magnitude of added noise on the timestep t. This trajectory progressively introduces incremental Gaussian noise $\mathcal{N}(\cdot)$, constructing a diffusion trajectory to corrupt x_{t-1} stepwisely. Consequently, the cumulative corruption gradually destroys original information, resulting in the final latent variable x_T that bears minimal resemblance to the original input x_0 .

The denoising part of the model counteracts the aforementioned process through learnable distributions $p_{\theta}(\mathbf{x}_{t-1}|\mathbf{x}_t)$ as:

$$p_{\theta}(\mathbf{x}_{t-1}|\mathbf{x}_t) = \mathcal{N}(\mathbf{x}_{t-1}; \boldsymbol{\mu}_{\theta}(\mathbf{x}_t, t), \boldsymbol{\Sigma}_{\theta}(\mathbf{x}_t, t)), \tag{2}$$

where $\mu_{\theta}(\cdot)$ and $\Sigma_{\theta}(\cdot)$ denote mean and covariance of learnable distribution by parameter θ , respectively. When the incremental noise added per diffusion step is sufficiently small, the denoising distributions can be sufficiently modeled as factorization across the data dimensions.

For optimization, diffusion models leverage variational inference and KL divergences to calculate the tractable posterior on x_0 :

$$\log p(\mathbf{x}_0) \ge \mathbb{E}_q [\log p(\mathbf{x}_0|\mathbf{x}_1) - KL(q(\mathbf{x}_T|\mathbf{x}_0)||p(\mathbf{x}_T)) - \sum_{t=2}^T KL(q(\mathbf{x}_{t-1}|\mathbf{x}_t,\mathbf{x}_0)||p(\mathbf{x}_{t-1}|\mathbf{x}_t))],$$
(3)

where $KL(q(\mathbf{x}_T|\mathbf{x}_0)||p(\mathbf{x}_T)) \approx 0$ can be omitted *iff.* the trajectory q has been well-defined [48]. For inference, diffusion models generate new data $\tilde{\mathbf{x}}_0$ from \mathbf{x}_T iteratively by the trained distribution p_θ .

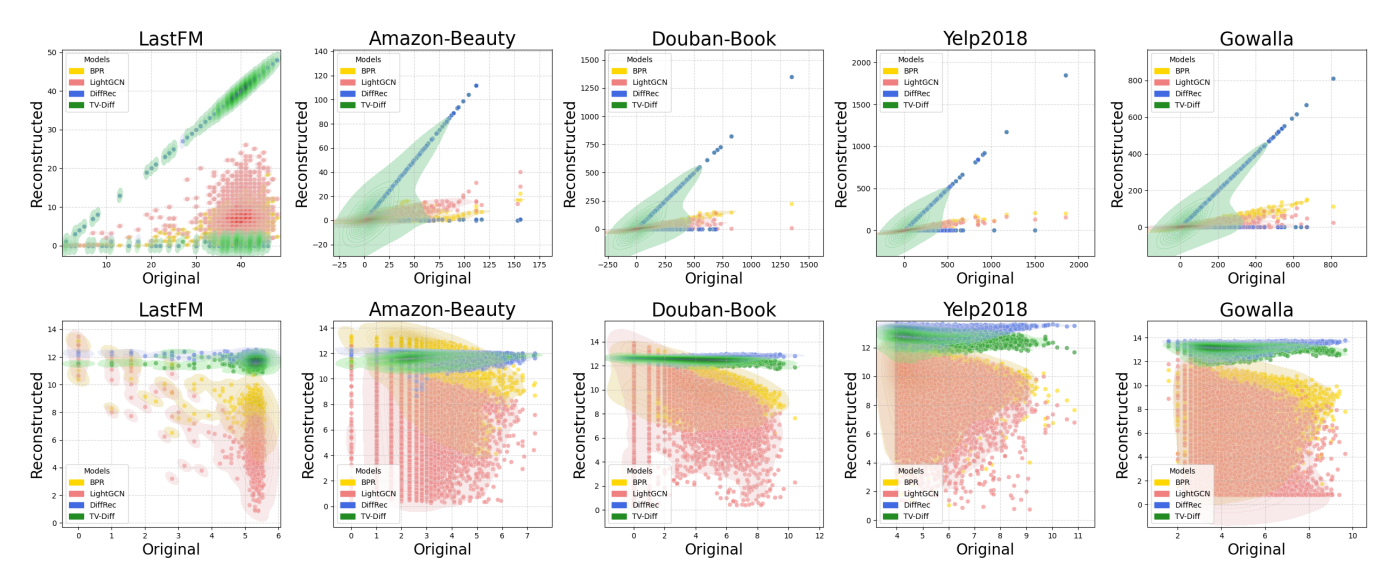


Figure 2: Visualization of Energy (upper) and Entropy (lower) on the user's original and reconstructed interaction probability.

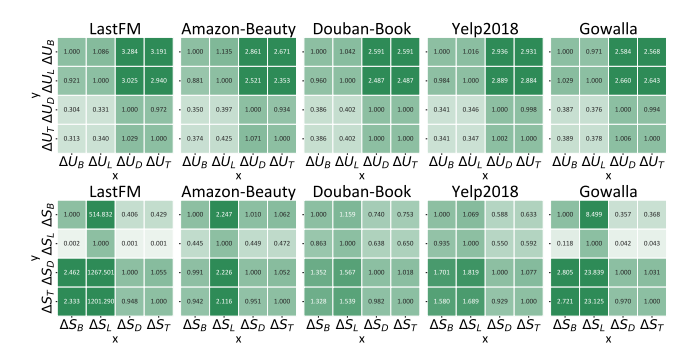


Figure 3: Detailed comparison among different models. $\Delta U_* \uparrow \in \mathbb{R}^-$ or $\Delta S_* \downarrow \in \mathbb{R}^+$ denotes the energy or entropy in difference on training, i.e., $U_*(\hat{\mathbf{R}}') - U_*(\hat{\mathbf{R}})$ or $S_*(\hat{\mathbf{R}}') - S_*(\hat{\mathbf{R}})$. The element in blocks denotes the $\frac{y}{x}$.

Tri-View Diffusion Recommendation Framework

Thermodynamic View - Helmholtz Free **Energy Maximization**

To investigate the completeness of DM-based recommender models and classic recommender models from a thermodynamic view, we choose three representative baselines, i.e., BPR[42], LightGCN [14], and DiffRec[55], to visualize the original users' interaction probability \hat{R} and the reconstructed ones \hat{R}' after training:

$$\hat{\mathbf{R}} = \mathbf{D}_{aI}^{-1} \mathbf{R},\tag{4}$$

$$\hat{\boldsymbol{R}} = \boldsymbol{D}_{\mathcal{U}}^{-1} \boldsymbol{R}, \tag{4}$$

$$\hat{\boldsymbol{R}}' = \begin{cases} \tilde{\boldsymbol{D}}_{\mathcal{U}}^{-1} \tilde{\boldsymbol{R}}, & \text{DiffRec} \\ Softmax(\boldsymbol{E}_{\mathcal{U}} \cdot \boldsymbol{E}_{\mathcal{I}}^{\top}), & \text{BPR, LightGCN} \end{cases}, \tag{5}$$

where $\tilde{\mathbf{R}} \in \mathbb{R}^{m \times n}$ denotes the raw reconstruction (a.k.a. *scores*), $m{D}_{\mathcal{U}} \in \mathbb{R}^{m \times m}$ and $m{\tilde{D}}_{\mathcal{U}} = diag(\frac{1}{\|m{\tilde{r}}_{1}\|_{1}}, \dots, \frac{1}{\|m{\tilde{r}}_{m}\|_{1}})$ denotes the original / reconstructed user degree matrix, $\|\cdot\|_{1}$ denotes the L1-norm, $E_{\mathcal{U}} \in \mathbb{R}^{m \times d}$ and $E_{\mathcal{I}} \in \mathbb{R}^{n \times d}$ are user / item representations, $Softmax(\cdot)$ denotes the row-wise softmax function. For clarity, we only take the acronym of model names hereafter. Note that this preprocessing step is implemented following their original prediction procedures, aiming to normalize users' interaction probabilities as a prerequisite for subsequent measurement. In terms of energy in thermodynamics, one of the most commonly used metrics is to measure the proportional number of interactions [12], so-called

explicit energy:
$$U(\hat{\mathbf{R}}') = tr(|\hat{\mathbf{R}}'|) \propto tr(\mathbf{D}_{\mathcal{U}}), \quad \hat{r}'_{u,i} := \begin{cases} 1, & \hat{r}'_{u,i} \ge \hat{r}_{u,i} \\ 0, & otherwise \end{cases}, \quad (6)$$

where $tr(\cdot)$ denotes the trace of a matrix. $|\hat{R}'| := (\hat{R}'\hat{R}'^*)^{\frac{1}{2}}$ where \hat{R}' is its conjugate transpose. However, such a strict classification would inevitably overlook those reconstructions that marginally fail the threshold, i.e., implicit energy. Hence, we fix the definition to involve both of them comprehensively:

$$U(\hat{\mathbf{R}}') = \sum_{u} \sum_{i} \mathbb{I}(\hat{r}'_{u,i} \ge r_{u,i}) + \mathbb{I}(\hat{r}'_{u,i} < r_{u,i}) \frac{\hat{r}'_{u,i}}{\hat{r}_{u,i}}, \tag{7}$$

where $\mathbb{I}(\cdot) = \{0, 1\}$ denotes the indication function. Specifically, the explicit energy refers to the potential links that are higher than the original probability, and the implicit energy means the weighted distance-based affinity. On the other hand, the equation of entropy is defined by Shannon Entropy for simplicity [44]:

$$S(\hat{\mathbf{R}}') = \sum_{u} -\hat{\mathbf{r}}'_{u} \log \hat{\mathbf{r}}'_{u}^{\top}.$$
 (8)

According to results on five datasets (cf. Figure 2 & Figure 3), we draw the following obvervations:

Observation 1. DM-based recommender models always preserves <u>higher</u> energy than the classic ones, i.e., $\frac{\Delta U_D}{\Delta U_{\{B,L\}}} \in (0,1)$.

It shows the connection between energy and the loss of diffusion models, which is commonly defined by the Mean Squared Error (MSE). By optimization, the reconstructed interaction matrix resembles the original one, with the increment of energy.

Observation 2. DM-based recommender models always fail to achieve <u>lower</u> entropy than the classic ones, i.e., $\frac{\Delta S_D}{\Delta S_{\{B,L\}}} > 1$. Specifically, DM-based recommender models are almost isentropic.

It shows the equivalence between *entropy* and the loss of classic recommender models, where BPR is employed in general. See the theoretical proof in Appendix B for details. However, none of the objectives in DM-based recommender models reflect the *entropy*.

Observation 3. Graph-based recommender model (i.e., LightGCN) exhibits stronger capability on entropy-reduction than its backbone (i.e., BPR), i.e., $\frac{\Delta S_B}{\Delta S_L} > 1$.

It attributes the significant decrease of *entropy* to the neighbors' information during message-passing. This effect is relevant to topological and anisotropic signals on the user-item bipartite graph, which will be discussed in detail in Section 3.2.

To sum up, DM-based recommender models and classic recommender models follow two independent optimization schemes, which reveal potential for a complete enhancement. To this end, we propose the *Helmholtz Free Energy* Maximization:

$$\mathcal{L}_{H}(\hat{\mathbf{R}}') \equiv \mathcal{L}_{U}(\hat{\mathbf{R}}') - t \cdot \mathcal{L}_{S}(\hat{\mathbf{R}}') = U(\hat{\mathbf{R}}') - t \cdot S(\hat{\mathbf{R}}')$$

$$= -\sum_{u \in \mathcal{B}} \sum_{i} (\hat{r}_{u,i} - \hat{r}'_{u,i})^{2}$$

$$- t \cdot (\hat{r}_{u,i} \log \sigma(\hat{r}'_{u,i}) - c_{u,i} \cdot (1 - \hat{r}_{u,i}) \log(1 - \sigma(\hat{r}'_{u,i}))),$$
(9)

where $\mathcal B$ denotes the user batch for training, t denotes the temperature, a coefficient to balance the priority of the two metrics. $\sigma(\cdot)$ denotes the sigmoid function. $c_{u,i} \in \{0,1\}$ denotes the confidence to sample the non-interactive items (See Section 3.3). The Helmholtz free energy expresses the maximum useful work extractable from a thermodynamic system given constant temperature. It reaches towards an equilibrium by maximizing energy and minimizing entropy in the meantime. Through the maximization of free energy, DM-based recommender models avert the collapse to suboptimal outcomes where entropy remains constant, leading to more generalized and robust results for personalization recommendations. It is worth noting that, Binary Cross Entropy (BCE) is intuitively adopted as the entropy-based loss due to its consistency with the user-wise computation on the energy-based loss. Nonetheless, alternative choices are also available, e.g., BPR, Negative Log Likelihood (NLL) that neglects the non-interactive class (i.e., $\hat{r}_{u,i} = 0$). We will compare their performance in Section 4.3.

3.2 Topological View - Anisotropic Denoiser

Based on Observation 3 in Section 3.1, we acknowledge that topological information, or graph structure, expresses rich relationships between users and items. The local and global neighborhoods are leveraged to exploit the connectivity patterns, e.g., anisotropy, centrality, and communities, for personalized recommendations. Specifically, the user-item bipartite graph is represented as $\mathcal{G}=(\mathcal{V},\mathcal{E})$, where $\mathcal{V}=\mathcal{U}\cup\mathcal{I}$ denotes all user and item nodes and \mathcal{E} denotes all the observed interactions between users and items. The symmetric normalized bipartite matrix without self-connection is defined as $\bar{R}=D_{\mathcal{U}}^{-\frac{1}{2}}RD_{\mathcal{I}}^{-\frac{1}{2}}$. Although topological information has been roughly adopted to DM-based recommender models, how the underlying anisotropy within the bipartite topology benefit to the optimization process of DM-based recommender models remain

unclear. In the context of *entropy*, we first arrive at a theorem that articulates its connection with topological information.

Lemma 3.1. Given a model trained on entropy (i.e., BPR), the optimal results approximate the bipartite matrix \mathbf{R} .

PROOF. The goal for BPR is to maximize the score estimator $s_{u,i+,i-} := s_{u,i+} - s_{u,i-}$ for all user-positive-negative triplets (u,i+,i-). When $s_{u,i+,i-} \to +\infty$, $s_{u,i+} \to +\infty$ and $s_{u,i-} \to -\infty$. After the activation function $\tilde{r}_{u,*} = \sigma(s_{u,*}) = 1/(1 + \exp^{-s_{u,*}})$, the optimal results are $\tilde{r}_{u,i+} = 1$ and $\tilde{r}_{u,i-} = 0$, which is the original binary interaction graph matrix R.

Theorem 3.2. Given a model trained on entropy (i.e., BPR), graph-based recommender models (i.e., LightGCN) with graph filter $\mathbf{D}_{\mathcal{U}}^{-\frac{1}{2}} \mathbf{R} \mathbf{D}_{I}^{-\frac{1}{2}}$ decreases more entropy during optimization, i.e., $\Delta S(\hat{\mathbf{R}}_{L}|\hat{\mathbf{R}}_{B}) \leq 0$.

PROOF. According to Lemma 3.1, the probabilistic matrix of BPR is $\hat{\pmb{R}}_B = \pmb{D}_{\mathcal{U}}^{-1} \pmb{R} = [r_{u,i}/d_u]_{m \times n} = [\hat{r}_{u,i}]_{m \times n}$, where d_u is the degree of user u. Similarly, LightGCN learns the graph structures by training, such that the prediction results approach to $\tilde{\pmb{R}}_L = \pmb{D}_{\mathcal{U}}^{-\frac{1}{2}} \pmb{R} \pmb{D}_I^{-\frac{1}{2}}$. After normalization for *entropy* calculation, the probabilistic matrix of LightGCN is $\hat{\pmb{R}}_L = \tilde{\pmb{D}}_{\mathcal{U}}^{-1} \tilde{\pmb{R}}_L = [r_{u,i}/(\sqrt{d_u}\sqrt{d_i})_{i}]_{m \times n}$, where d_i and d_j denotes the degree of item i and j, respectively. Hence, the pivotal point of proof lies in the calculation of the difference between $S(\hat{\pmb{R}}_B)$ and $S(\hat{\pmb{R}}_L)$:

$$\Delta S(\hat{\mathbf{R}}_{L}|\hat{\mathbf{R}}_{B}) = S(\hat{\mathbf{R}}_{L}) - S(\hat{\mathbf{R}}_{B})$$

$$= \sum_{u} \sum_{i} -\hat{r}'_{u,i} \log \hat{r}'_{u,i} + \hat{r}_{u,i} \log \hat{r}_{u,i}.$$
(10)

After simplifying the equation, we have:

$$\Delta S(\hat{\mathbf{R}}_{L}|\hat{\mathbf{R}}_{B}) = \sum_{u} \sum_{i} - \frac{r_{u,i}}{\sqrt{d_{i}} \sum_{j} (r_{u,j}/\sqrt{d_{j}})} \log r_{u,i}$$

$$+ \frac{r_{u,i}}{\sqrt{d_{i}} \sum_{j} (r_{u,j}/\sqrt{d_{j}})} \log(\sqrt{d_{i}} \sum_{j} (r_{u,j}/\sqrt{d_{j}})) - \frac{r_{u,i}}{d_{u}} \log d_{u}$$

$$= \sum_{u} \sum_{i} r_{u,i} \left(\frac{\log(\sqrt{d_{i}} \sum_{j} (r_{u,j}/\sqrt{d_{j}})}{\sqrt{d_{i}} \sum_{j} (r_{u,j}/\sqrt{d_{j}})} - \frac{\log d_{u}}{d_{u}} \right)$$

$$= \sum_{u} (\|[-\frac{1}{\sqrt{d_{i}} \sum_{j} (r_{u,j}/\sqrt{d_{j}})} \log \frac{1}{\sqrt{d_{i}} \sum_{j} (r_{u,j}/\sqrt{d_{j}})}]_{d_{u}}\|_{1}$$

$$- \|[-\frac{1}{d_{u}} \log \frac{1}{d_{u}}]_{d_{u}}\|_{1}) \le 0 \quad \text{subject to } \forall i \in N(u), \quad (12)$$

where $\|\cdot\|_1$ denotes L1-norm. The first term of the primary equation (cf. Eq. (11)) becomes 0 for $r_{u,*} \in \{0,1\}$. Since the second term of the final equation (cf. Eq. (12)) achieves the maximum *entropy* for interactive-item vectors $[\cdot]_{d_u}$, the *entropy* difference between the two models is always non-positive. Hence, though as a low-pass filter, \bar{R} attains \underline{NO} smoother item probability counterintuitively.

Remark. In general, energy and entropy act as countervailing forces, akin to DM-based versus classic recommender models. However, though Theorem 3.2 posits lower entropy for LightGCN, its implementation of multi-layer message-passing potentially explores non-interactive items. Thus, LightGCN might paradoxically result in higher overall energy (cf. Figure 3). Noting that, message-passing

with more layers inevitably increases entropy (See Appendix C), necessitating a trade-off consideration on the total number of layers.

To sum up, incorporating item degree information into the topology facilitates *entropy*-based training objective to achieve higher *Helmholtz free energy* via *entropy* reduction, eventually improving model performance. Furthermore, the inconsistency between user and item degree distribution, which is the exclusive anisotropy inherent to user-item bipartite graphs, necessitates an asynchronous modeling. To this end, we propose the anisotropic denoiser:

$$\tilde{\mathbf{x}}_{\theta}(\mathbf{x}_{t}, t) = \mathbf{h}_{u|\theta}(\mathbf{x}_{t}, t) \cdot \mathbf{H}_{I|\theta}(\mathbf{x}_{t}, t)^{\top}$$

$$= \tanh(Agg(\mathbf{x}_{t} \cdot \mathbf{W}_{I}, \mathbf{e}_{t})) \cdot \tanh(\bar{\mathbf{R}}^{\top} \cdot \mathbf{W}_{\mathcal{U}})^{\top},$$
(13)

$$\hat{\mathbf{r}}_{u}' = \tilde{\mathbf{x}}_{\theta}(\mathbf{x}_{t}, t) / \|\tilde{\mathbf{x}}_{\theta}(\mathbf{x}_{t}, t)\|_{1}, \tag{14}$$

where $W_I \in \mathbb{R}^{n \times d}$, $W_{\mathcal{U}} \in \mathbb{R}^{m \times d}$ denotes the latent transformation matrices, $e_t \in \mathbb{R}^d$ denotes the learnable time embedding. $\bar{R} \in \mathbb{R}^{m \times n}$ denotes the symmetric normalized bipartite matrix. $Agg(\cdot)$ denotes the aggregation function, e.g., element-wise addition. $tanh(\cdot)$ is the activation functions as [55]. In conclusion, the user-wise encoderdecoder paradigm in existing DM-based approaches solely models the user degree distribution and presumes the item degree distribution in line with it. In contrast, the anisotropic denoiser explicitly accounts for the item degree on explicit topological information and drives predictions by calculating the user-item cross-correlation. According to Theorem 3.2, we only involve single-layer messagepassing to preserve anisotropic signals and avoid loss of entropy from multi-layer message-passing. It also saves computational resources, particularly on pre-training or multi-layer message-passing on large graphs constructed from large datasets. Consequently, TV-Diff can obviate complex and sometimes redundant efforts in capturing anisotropic signals.

3.3 Hard-Negative View - Acceptance-Rejection Gumbel Sampling Process

The maximization of Helmholtz free energy integrates both genres of objectives for optimization. It necessitates an efficient yet effective negative sampling method to ensure the consistent robustness of their mutual joint-training. However, the abundance of non-interactive items overwhelms the distribution of positive items when the model is trained on the entire itemset, deteriorating the model's efficacy and efficiency. The confidence $c_{u,i}$ ~ $Bernoulli(\frac{N(u)}{n})$ is thus introduced to balance the far-outnumbered non-interactive items, through which the model randomly samples negative items at a rate proportional to the number of interactions [42]. Although hard negative sampling (Hard NS) methods [39, 62] retrieve high-quality informative negative items, capture informative semantics, and accelerate convergence during training, they impose the negative distribution $p_n(j|u)$ sub-linearly correlated to the positive $p_d(i|u)$, are not judicious for the recommendation tasks on the bipartite interaction graph. By corroborating this understanding, we delve into the negative distribution on one of the simplest recommender models (i.e., BPR) with its score estimator $s_{u,*}$:

Theorem 3.3. The expected loss of BPR reaches the upper bound if and only if $p_n(j|u) = C \cdot p_d(i|u)$, and the lower bound if $p_n(j|u) \cdot p_d(i|u) = 0$ for all positive-negative item pair (i, j).

PROOF. The objective function for each user u is

$$\mathcal{L}_{BPR}(u) = \mathbb{E}_{i \cdot p_d(u)} \mathbb{E}_{j \cdot p_n(u)} \left[-\log \sigma(\boldsymbol{e}_u \boldsymbol{e}_i^{\mathsf{T}} - \boldsymbol{e}_u \boldsymbol{e}_j^{\mathsf{T}}) \right]$$

$$= \sum_{i} p_d(i|u) \sum_{j} p_n(j|u) \left[-\log \sigma(s_{u,i} - s_{u,j}) \right]$$

$$\leq \sum_{i} \sum_{j} \left[-\log \sigma(s_{u,i} - s_{u,j}) \right],$$
(15)

where $\sum_i p_d(i|u) = \sum_j p_n(j|u) = 1$, and the upper bound (cf. Eq. (15)) holds according to Cauchy–Schwarz Inequality. The maximizer satisfies $p_n(j|u) = C \cdot \mathbb{E}[-\log \sigma(s_{u,i} - s_{u,j})]$, where C denotes the constant. Conversely, the minimizer of $\mathcal{L}_{BPR}(u)$ arrives at 0 if it adheres to the condition that they are orthogonal. The same applies to $p_d(i|u)$. Therefore, when the positive and negative distributions are correlated in a sub-linear manner, BPR loss will compromise amid optimization (orthogonality) - generalization (linearity). The same issue arises in BCE due to their equivalence to entropy-based losses. In contrast to previous work that imposes the negative and positive distribution sub-linearly correlated, enforcing orthogonality between them preserves informative semantics (e.g., anisotropy) for the training of the denoiser.

To properly sample hard negatives deviated from positives, we adopt the acceptance-rejection sampling [10] to truncate the potentially non-informative items:

$$c_{u,j} \sim p_n(j|u) \approx \begin{cases} \frac{1}{\gamma \cdot n}, & \operatorname{Rank}(\tilde{r}_{u,j}) \leq \gamma \cdot n \\ \epsilon, & \operatorname{Rank}(\tilde{r}_{u,j}) > \gamma \cdot n \end{cases}$$
 (16)

where $\gamma \in (0,1]$ denotes the negative factor controlling the threshold of informative negatives, ϵ denotes the infinitesimal, and Rank(·) denotes the function that returns the position of item j in the monotonically decreasing-order list of all items scores $\tilde{r}_{u,*} \propto s_{u,*}$. However, in DM-based recommender models, the scores can be unreliable: When large diffusion timesteps are sampled, the forward process will overcorrupt the input. It severely challenges the denoiser's capability in the reverse process, barely reconstructing the scores accurately. As a result, the Hard-NS method struggles in distinguishing negatives and degrades model performance due to false negatives. To address this issue, we apply a timestep-dependent Gumbel Softmax on top of acceptance-rejection sampling:

$$\hat{p}_{n}(j|u) = Softmax(\frac{\log p_{n}(j|u) + g_{j}}{\tau(\bar{t})}) = \frac{\exp(\frac{\log p_{n}(j|u) + g_{j}}{\exp(-\lambda \bar{t})})}{\sum_{j'} \exp(\frac{\log p_{n}(j'|u) + g_{j'}}{\exp(-\lambda \bar{t})})},$$
(17)

where $g \sim Gumbel(0,1)$ is sampled by the reparameterization trick, i.e., $g = -\log(\log(\mu)), \mu \sim Uniform(0,1)$. λ denotes the relaxation rate of Hard NS. $\bar{t} = 1 - \frac{t}{T}$ ensures that when $t \to T$, $\tau(\bar{t}) \to 1$ reaches the maximum, and the negative distribution towards a uniform distribution among all items to avoid mistakes of negatives. Altogether, the Acceptance-Rejection Gumbel Sampling Process (AR-GSP) establishes a dual-aspect Hard-NS strategy: On the general recommendation aspect, acceptance-rejection sampling manageably dissects the item pool into positives and long-tailed true negatives [67]. Then, true positives and false positives (i.e., hard negatives) contribute evenly to the model's generalization. On the diffusion aspect, the time-dependent Gumbel-Softmax is a DM-specific approach that assesses the reliability of the preliminary negative distribution and adaptively provides a viable one.

Table 1: Overall performance comparison with representative models on five datasets. For acronyms used in Type, "B" represents base recommenders; "A" refers to autoencoder-based recommenders; "G" means the graph-based recommenders; "N" means the negative sampling recommenders; "D" represents diffusion-based recommenders.

	Dataset		Las	tFM			Amazon	-Beauty			Douba	n-Book			Yelp	2018			Gov	walla	
Type	Method	R@10	N@10	R@20	N@20	R@10	N@10	R@20	N@20	R@10	N@10	R@20	N@20	R@10	N@10	R@20	N@20	R@10	N@10	R@20	N@20
В	BPR-MF	0.1742	0.2070	0.2602	0.2435	0.0711	0.0470	0.1015	0.0572	0.0776	0.0927	0.1268	0.1038	0.0279	0.0316	0.0491	0.0397	0.1045	0.1052	0.0456	0.1213
	NeuMF	0.1454	0.1669	0.2257	0.2056	0.0622	0.0397	0.0937	0.0496	0.0572	0.0673	0.0895	0.0735	0.0224	0.0250	0.0396	0.0314	0.0932	0.0904	0.1398	0.1051
A	CDAE	0.0752	0.0877	0.1082	0.0906	0.0208	0.0119	0.0341	0.0157	0.0463	0.0508	0.0716	0.0579	0.0073	0.0081	0.0127	0.0102	0.0209	0.0190	0.0305	0.0210
	MultiVAE	0.1040	0.1220	0.2713	0.2488	0.0576	0.0391	0.1018	0.0574	0.0459	0.0475	0.1207	0.1008	0.0245	0.0271	0.0542	0.0434	0.0763	0.0711	0.1480	0.1121
G	LightGCN	0.1980	0.2347	0.2999	0.2836	0.0921	0.0596	0.1308	0.0735	0.1000	0.1161	0.1504	0.1264	0.0342	0.0390	0.0587	0.0482	0.1278	0.1297	0.1857	0.1474
	ChebyCF	0.1868	0.2261	0.2981	0.2853	0.0839	0.0595	0.1358	0.0795	0.1107	0.1245	0.1762	0.1644	0.0348	0.0398	0.0598	0.0495	0.1318	0.1323	0.2002	0.1577
	LinkProp	0.1182	0.1446	0.2763	0.2647	0.0884	0.0648	0.1202	0.0747	0.0929	0.1088	0.1727	0.1513	0.0352	0.0402	0.0635	0.0517	0.1263	0.1261	0.2084	0.1642
	SGCL	0.1899	0.2305	0.3093	0.2946	0.1004	0.0678	0.1433	0.0810	0.1405	0.1704	0.1939	0.1771	0.0416	0.0472	0.0679	0.0555	0.1498	0.1516	0.2172	0.1705
N	MixGCF	0.1935	0.2306	0.3009	0.2838	0.0933	0.0607	0.1356	0.0754	0.0940	0.1104	0.1502	0.1242	0.0334	0.0378	0.0621	0.0509	0.1248	0.1254	0.1959	0.1542
	AHNS	0.1921	0.2285	0.2744	0.2611	0.0905	0.0583	0.1427	0.0802	0.1285	0.1633	0.1839	0.1690	0.0366	0.0422	0.0631	0.0519	0.1160	0.1183	0.1724	0.1346
D	CODIGEM DiffRec BSPM GiffCF DDRM HDRM	0.2122 0.2127 0.1962 0.1735 0.1966 0.1807	0.2530 0.2538 0.2349 0.2112 0.2337 0.2139	0.2943 0.2985 0.2852 0.2582 0.2815 0.2951	0.2831 0.2867 0.2708 0.2501 0.2675 0.2782	0.0666 0.0850 0.0814 0.0673 0.0949 0.0667	0.0478 0.0586 0.0602 0.0488 0.0627 0.0438	0.0916 0.1206 0.1405 0.1019 0.1365 0.1300	0.0556 0.0713 0.0797 0.0620 0.0760 0.0695	0.1115 0.1356 0.1296 0.0502 0.0830 0.0769	0.1454 0.1682 0.1594 0.0578 0.0957 0.0914	0.0716 0.1847 0.1843 0.1586 0.1272 0.1281	0.0563 0.1695 0.1740 0.1344 0.1065 0.1080	$0.0349 \\ 0.0380 \\ \underline{0.0401} \\ 0.0327 \\ 0.0328 \\ 0.0217$	0.0407 0.0443 0.0455 0.0394 0.0377 0.0257	0.0590 0.0603 0.0670 0.0642 0.0556 0.0404	0.0491 0.0506 0.0553 0.0529 0.0457 0.0332	0.0930 0.1383 0.1484 0.1371 0.1147 0.0800	0.0997 0.1439 0.1498 0.1397 0.1163 0.0773	0.1347 0.1981 0.2023 0.1885 0.1674 0.1293	0.1099 0.1593 0.1577 0.1470 0.1317 0.0959
-	TV-Diff	0.2220	0.2605	0.3133	0.2953	0.1046	0.0719	0.1475	0.0852	0.1474	0.1863	0.2037	0.1908	0.0416	0.0481	0.0700	0.0582	0.1517	0.1578	0.2195	0.1762
	Imp. (Follow-up)	4.37%	2.64%	1.29%	0.24%	4.18%	6.05%	2.93%	5.19%	4.91%	9.33%	5.05%	7.74%	0.00%	1.91%	3.09%	4.86%	1.27%	4.09%	1.06%	3.34%
	Imp. (DiffRec)	4.37%	2.64%	4.96%	3.00%	23.06%	22.70%	22.31%	19.50%	14.71%	10.76%	10.27%	12.57%	9.47%	8.58%	16.09%	15.02%	9.69%	9.66%	10.80%	10.61%

4 Experiments

4.1 Experimental Settings

Table 2: Statistics of experimental data.

Dataset	#User	#Item	#Interaction	%Density
LastFM	1,892	17,632	92,834	0.2783
Amazon-Beauty	22,364	12,102	198,502	0.0733
Douban-Book	13,024	22,347	792,062	0.2721
Gowalla	29,858	40,981	1,027,370	0.0840
Yelp2018	31,668	38,048	1,561,406	0.1296

Datasets. We use five real-world datasets to evaluate the performance of TV-Diff, including *Lastfm*¹, *Amazon-Beauty*², *Douban-Book*², *Gowalla*³ and *Yelp2018*² for overall comparisons. These datasets are publicly available and have been widely used in various literature [2, 5, 14, 55, 56, 65]. All ratings are binarized as implicit feedback. We randomly split the datasets into training sets and test sets with a proportion of 8:2.

Metrics. We use two popular evaluation metrics for Top-K recommendations: Recall@K (R@K) and NDCG@K (N@K), where $K \in \{10, 20\}$. We highlight the best method in boldface and underline the follow-up one. In our work, a relative improvement above 1% is considered significant [45].

Baselines. We conduct experiments by comparing a series of representative recommender models (RMs), categorized into five types: Base RM utilizes its ability to simply extract collaborative signals on the user-item interactions: BPR-MF [42], NeuMF [15]; Autoencoder-based RM learns compressed representations and reconstructs incomplete interactions by an encoder and a decoder respectively: CDAE [57], MultiVAE [34]; Graph-based RM mainly focus on the message-passing mechanism and their efficiency on

graphs: LightGCN [14], ChebyCF [24]; LinkProp [8], SGCL [69]. Negative Sampling RM aims to sample or synthesize informative negative items from the large item pool: MixGCF [21], AHNS [29]; Diffusion-based RM leverages iterative corruption and denoising to model a refined user preference: CODIGEM [54], DiffRec [55], BSPM [5], GiffCF [71], DDRM [18], HDRM [66].

Implementation Details. For a fair comparison, we use grid search to fine-tune all the hyperparameters of the baselines within the intervals reported in the original papers, and assign the same threshold of early-stopping (i.e., 10 [55]) for all models. For the general settings, we fix a series of hyperparameters for all comparison methods: the latent size is set to 64, the coefficient of regularization is fixed to 1*e*–4, the relaxation rate is empirically set to 3 [50], and the number of inference timesteps is equal to the training timesteps [55]. We use the Xavier method [11] to initialize all parameters, and Adam [25] to optimize all these models. For fair negative sampling evaluations, we uniformly pair a positive item with one negative item for each training iteration [42]. To reproduce the results, we fix the random seed to 0 in PyTorch. For more detailed information, please refer to the source code ⁴.

4.2 Performance Comparison

In this section, we compare our TV-Diff with the five different kinds of recommender models. Improvements compared to the follow-up models and the backbone DiffRec are also highlighted for inference. According to the experimental results, we can obtain the following observations:

• TV-Diff consistently yields the best performance on all datasets in terms of all evaluation metrics (cf. Table 1). This demonstrates that TV-Diff is capable of distilling, modeling, and generating comprehensive user preferences. We advocate that TV-Diff bestows a holistic diffusion recommendation framework via (1) a complete

 $^{^{1}} https://github.com/librahu/HIN-Datasets-for-Recommendation-and-Network-Embedding \\$

²https://github.com/Coder-Yu/SELFRec

 $^{^3} https://github.com/xiangwang 1223/neural_graph_collaborative_filtering$

⁴https://github.com/umsimonchen/TV-Diff

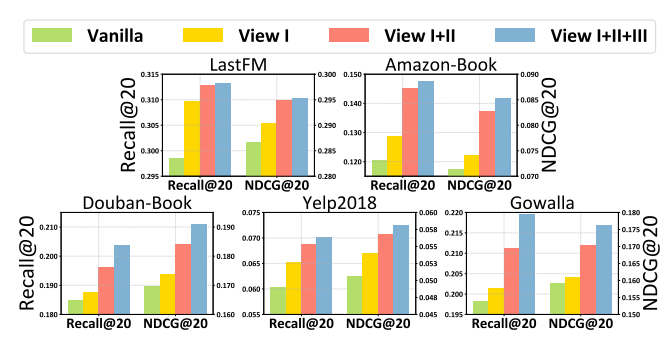


Figure 4: Ablation study on different views.

optimization objective, (2) a bipartite-graph-specific denoiser, and (3) an adaptive DM-based hard negative sampling strategy.

- DM-based recommender models exhibit superior performance over autoencoder-based models, attributable to their distinctive denoising score matching mechanism. Specifically, TV-Diff achieves significant improvements, averaging over 12%, compared to existing DM-based approaches. These gains demonstrate the ability of TV-Diff to overcome inherent limitations from the thermodynamic and topological views, which hinder diffusion models from attaining optimal results. Furthermore, by eliminating the need for pre-training, TV-Diff mitigates the instability that is highly sensitively associated with the quality of pre-trained embeddings.
- We acknowledge the admirable performance of the contrastive learning approach, which consistently achieves competitive results as a follow-up model. However, its capability is widely attributed to batch-wise negative sampling, leveraging multiple negatives to capture comprehensive semantics. Notably, TV-Diff outperforms the contrastive learning and negative sampling approaches with an average improvement exceeding 3.5%. This result suggests that our proposed hard negative sampling strategy effectively identifies the most informative negative while preventing redundant batch-wise negative sampling and their computations.

4.3 Ablation Analysis

Effectiveness of Different Views. We first analyze the interplay and contributions of TV-Diff's components. Specifically, View I, II, and III denote the *Helmholtz Free Energy* maximization, anisotropic denoiser, and acceptance-rejection Gumbel sampling process (AR-GSP), respectively. The ablated models are evaluated incrementally, corresponding to the framework's progressive development: *Helmholtz Free Energy* maximization serves as the core foundation; the *entropy*-based objective subsequently enlightens the anisotropic denoiser; and finally, the training process of the denoiser is intertwined with AR-GSP in terms of the reconstruction and semantics. Vanilla refers to the backbone model DiffRec, without any proposed view, and View I+II+III represents our complete framework.

From the results, we observe that incorporating newly different components based on the previous ablated models leads to significant performance improvements across all base models (cf. Table 4). This confirms that each component is crucial to TV-Diff. On one hand, the anisotropic denoiser achieves the highest gains among most datasets. For example, View I+II outperforms its counterpart View I by over 8% on average. On the other hand, AR-GSP achieves only over 3% improvements, and even less on smaller datasets (e.g.,

LastFM). These findings provide compelling evidence that the existing DM-based recommender models are markedly ineffective in capturing anisotropy among bipartite graphs, while their outstanding denoising ability somehow diminishes the need for hard negative sampling, thereby saving computational resources.

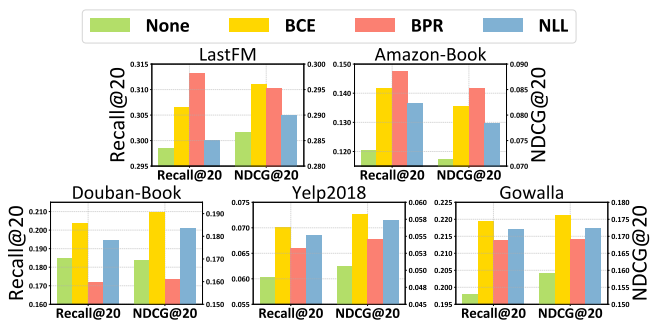


Figure 5: Ablation study on entropy-based objectives.

Impact of *Entropy*-Based Objectives. Three widely used *entropy*-based training objectives (i.e., BCE, BPR, NLL) are evaluated against a control group (i.e., None). The results (cf. Figure 5) show that *entropy*-based objectives consistently enhance the performance compared to solely employing *energy*-based objectives. Furthermore, our observations indicate that small datasets favor BPR, whereas large datasets favor BCE. We hypothesize that the triplet formulation in BPR provides more nuanced user preferences from limited interactions, but may induce overfitting and deteriorate generalization if given abundant interactions.

Table 3: Ablation study on Acceptance-Rejection Sampling (AR) compared with Sub-Linear Correlation (SL).

Dataset	Method	R@10	N@10	R@20	N@20
LootEM	w/ SL	0.2098	0.2419	0.3022	0.2895
LastFM	w/ AR	0.2165	0.2533	0.3108	0.2925
Douban	w/ SL	0.1274	0.1431	0.1768	0.1545
Douban	w/ AR	0.1353	0.1587	0.1832	0.1692
Carralla	w/ SL	0.1318	0.1375	0.2072	0.1627
Gowalla	w/ AR	0.1437	0.1459	0.2178	0.1721

Comparison of Acceptance-Rejection sampling and Traditional Hard NS. To rigorously evaluate the superiority of the acceptance-rejection sampling (AR) over the conventional sublinear correlation (SL) in recommendation tasks, we conduct a direct comparison under identical conditions, where both sample one negative item across the entire item sets. For clarity in causal analysis, we employ LightGCN as the base model due to its concise architecture. Our results (cf. Table 3) state that AR consistently and significantly outperforms SL, where the improvements notably exceed even 10% on Douban-Book. These findings highlight AR's superior efficacy in learning latent semantics within recommendation tasks and underscore the importance of truncating true negatives during sampling, particularly for long-tail distributions.

Hyperparameter Sensitivity Analysis for Temperature t. We analyze the sensitivity of the key hyperparameter: temperature t. This parameter controls the priority between *energy* and *entropy* for the maximization of *Helmholtz free energy*. We vary t in the range $\{0.1, 0.5, 1, 5, 10, 15\}$. According to the results (cf. Figure 6), TV-Diff reaches a peak when t = 1 for small datasets and t = 10 for

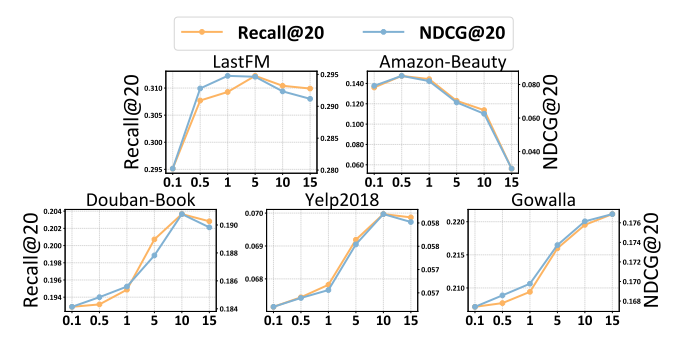


Figure 6: Influence of the temperature t.

large datasets. This phenomenon suggests balanced optimization strategies are more preferable for small datasets, while greater importance should be assigned to *entropy*-based objectives for large datasets, given the inherent sparsity per user/item of datasets.

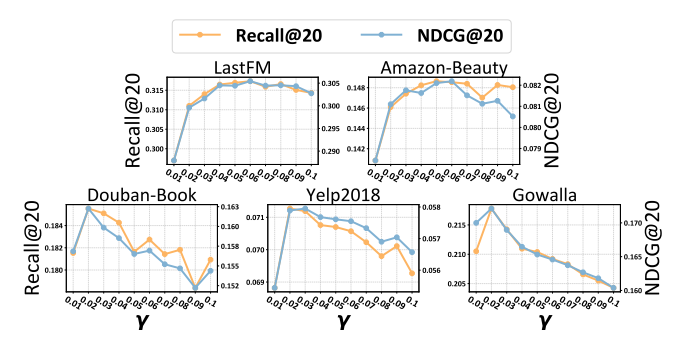


Figure 7: Influence of the negative factor γ .

Hyperparameter Sensitivity Analysis for Negative Factor γ .

We also analyze the sensitivity of the negative factor γ . This parameter controls both the number and position of candidate negative items within the entire itemset. Hyperparameter y is ranged in [0.01, 0.1] in increments of 0.01. The findings indicate that TV-Diff's performance consistently improves across all datasets as y increases, reaches a peak, and then gradually declines (cf. Figure 7). On one side, small datasets benefit from $\gamma = 0.5$ to avoid representation collapse. On the other side, large datasets achieve the best performance when $\gamma = 0.2$, reflecting their need for few but informative negatives following a long-tail distribution. It is worth noting that, when γ becomes too small, performance declines sharply, suggesting items with higher recommendation scores may inadvertently include unobserved positive samples. Thus, to mitigate biased selection based on recommendation scores, this observation underscores the rationale for applying uniform sampling on candidate negative items after the completion of AR, as in our implementation.

Case Study for Visualization of Energy and Entropy. Following the pilot experiments, we visualize the reconstructed interaction probability in terms of energy and entropy. According to Figure 2 and 3, we recognize that, as a DM-based recommendation framework, TV-Diff aligns with mainstream approaches in prioritizing energy maximization. Nonetheless, TV-Diff exhibits a superior capability to minimize the entropy compared to DiffRec, i.e., $\frac{\Delta S_D}{\Delta S_T} > 1$. These results illustrate that TV-Diff transcends the limitation of a unilateral training objective, reconciles both factors via free energy, and attains enhanced generalization and performance.

Table 4: Efficiency comparison. UT denotes the Unit Time per epoch; Ep. denotes the training Epoch; K denotes layers; $|R|^+$ denotes the non-zero values of the graph.

	Light	GCN	Diff	Rec	TV-Diff		
(s=second)	UT↓	#Ep.↓	UT↓	#Ep.↓	UT↓	#Ep.↓	
LastFM	0.623s	424	0.353s	46	1.056s	26	
Douban	5.345s	270	2.572s	66	1.649s	42	
Gowalla	14.748s	368	19.303s	113	5.162s	45	
Space	O((m -	+ n)d)	O((m -	+ n)d)	O((m+n)d)		
Time	$O(R^+ $	[<i>Kd</i>)	O(2n	nnd)	$O(\mathcal{B} nd + \mathbf{R}^+ d)$		

Efficiency Analysis. For evaluations, LightGCN and DiffRec are chosen due to their simplest architecture. We run all on an Intel(R) Core(TM) i7-12700 CPU and a GeForce RTX 3090 GPU. According to the analysis (cf. Table 4), TV-Diff is fairly efficient, especially on large datasets where LightGCN suffers from multi-layer message-passing on large graphs and DiffRec fails to maintain performance from batch-training. Notably, the ranking for AR-GSP occupied $O(|\mathcal{B}|n\log n)$, which can be omitted.

5 Related Work

5.1 Diffusion-based Recommender Models

Diffusion models are viewed as extensions of flow models [43], autoencoders [1], and variational autoencoders [26], architecturally evolving single discrete encoder/decoder steps into multiple continuous diffusion steps. From an optimization perspective, they also draw upon deep energy-based models [51], score-based models (SBMs) [22], and denoising SBMs [53] to maximize the likelihood in a more tractable and efficient manner. Inspired by the breakthroughs of [18, 19, 35, 48], diffusion models have recently been applied to general recommendation tasks [54, 55] and demonstrated their outstanding potential. However, early diffusion-based recommender models overlook the topology information inherent in bipartite interaction graphs, a consideration largely irrelevant in the field of computer vision. To address this, BSPM [5], GiffCF [71], and S-Diff [59] simulate the message-passing within the diffusion process. Additionally, a two-stage training strategy [66, 70] also facilitates graph structures learning during pre-training and high-quality representation retrieval via diffusion-based fine-tuning. Nevertheless, this approach incurs substantially higher computational costs than end-to-end training.

5.2 Graph-based Recommender Models

With the rapid development of graph neural networks (GNNs) [13, 27, 52], graph-based recommendation models have become thriving [14, 64]. Generally, four mainstream approach prevail: (1) Graph Signal Processing [24, 37, 40] methods leveage Graph Fourier Transform and low-pass filters to extract low-frequency collaborative signals embedded in graph structures; (2) Hypergraph methods [3, 23, 58] construct hypergraphs to explore richer collaborative filtering architectures capable of modeling higher-order ralationships; (3) Negative Sampling methods [21, 28, 29] focus on identifying the underlying negative distribution and maximizing the distiction between positive and negative items by exploiting graph structures; (4) Contrastive Learning models [2, 56, 69] harness alignment and

uniformity of representations across augmented graph views to mitigate the data sparsity. However, these methods rely on the multi-layer message-passing for noise smoothing and feature extraction, bearing substantial overhead on massive graphs.

5.3 Hard Negative Sampling

As a necessary component in recommender systems, negative sampling critically impacts recommendation outcomes [61]. The most common approach, Random Negative Sampling (RNS) [42], often involves irrelevant items during training. This limitation has motivated the development of Hard Negative Sampling (Hard NS), which prioritizes informative negative items. Theoretical analyses for link prediction tasks indicate that hard negative distributions should exhibit sub-linear correlation with positive distributions [7, 21, 29, 39, 62]. However, applying this principle to BPR can be problematic: it risks deteriorating the pairwise loss into a pointwise objective, potentially leading to worse performance. In this work, we pioneer the exploration of hard negative sampling in the context of diffusion-based recommendation tasks.

6 Conclusion

In this work, we introduce **TV-Diff**, a novel tri-view diffusion recommendation framework designed to address the limitations of DM-based recommender models. By leveraging the *Helmholtz free energy maximization*, TV-Diff optimizes recommender models by both *energy* and *entropy*, where the robustness of the joint-training is guaranteed by the anisotropic denoiser and acceptance-rejection Gumbel sampling process. The former captures nuances between user and item degree distributions and reconstructs predictions by user-item cross-correlation with explicit topology information, while the latter provides informative negatives for DM-based recommender models. In the future, we will delve into the fundamental architecture and process of DMs for better recommendations.

Acknowledgments

This work was supported by The Science and Technology Development Fund, Macau SAR (0126/2024/RIA2, 001/2024/SKL), CG-2026, GDST (2020B1212030003, 2023A0505030013), Nansha District (2023ZD001), MYRG-GRG2023-00186-FST-UMDF, MYRG-GRG2025-00234-FST.

References

- Pierre Baldi. 2012. Autoencoders, Unsupervised Learning, and Deep Architectures. In Proceedings of ICML Workshop on Unsupervised and Transfer Learning (Proceedings of Machine Learning Research, Vol. 27), Isabelle Guyon, Gideon Dror, Vincent Lemaire, Graham Taylor, and Daniel Silver (Eds.). PMLR, Bellevue, Washington, USA, 37–49.
- [2] Xuheng Cai, Chao Huang, Lianghao Xia, and Xubin Ren. 2023. LightGCL: Simple Yet Effective Graph Contrastive Learning for Recommendation. In The Eleventh International Conference on Learning Representations.
- [3] Ximing Chen, Pui Ieng Lei, Yijun Sheng, Yanyan Liu, and Zhiguo Gong. 2024. Social Influence Learning for Recommendation Systems. In Proceedings of the 33rd ACM International Conference on Information and Knowledge Management (CIKM '24). New York, NY, USA.
- [4] Heng-Tze Cheng, Levent Koc, Jeremiah Harmsen, Tal Shaked, Tushar Chandra, Hrishi Aradhye, Glen Anderson, Greg Corrado, Wei Chai, Mustafa Ispir, Rohan Anil, Zakaria Haque, Lichan Hong, Vihan Jain, Xiaobing Liu, and Hemal Shah. 2016. Wide & Deep Learning for Recommender Systems. In Proceedings of the 1st Workshop on Deep Learning for Recommender Systems (Boston, MA, USA) (DLRS 2016). Association for Computing Machinery, New York, NY, USA, 7-10.
- [5] Jeongwhan Choi, Seoyoung Hong, Noseong Park, and Sung-Bae Cho. 2023. Blurring-Sharpening Process Models for Collaborative Filtering. In Proceedings

- of the 46th International ACM SIGIR Conference on Research and Development in Information Retrieval (Taipei, Taiwan) (SIGIR '23). Association for Computing Machinery, New York, NY, USA, 1096–1106.
- [6] Willem Van den Heuvel and Alessandro Soncini. 2012. NMR chemical shift as analytical derivative of the Helmholtz free energy. The Journal of chemical physics 138 5 (2012), 054113. https://api.semanticscholar.org/CorpusID:24047674
- [7] Jingtao Ding, Yuhan Quan, Quanming Yao, Yong Li, and Depeng Jin. 2020. Simplify and robustify negative sampling for implicit collaborative filtering. In Proceedings of the 34th International Conference on Neural Information Processing Systems (NIPS '20).
- [8] Hao-Ming Fu, Patrick Poirson, Kwot Sin Lee, and Chen Wang. 2022. Revisiting Neighborhood-based Link Prediction for Collaborative Filtering. In Companion Proceedings of the Web Conference 2022 (Virtual Event, Lyon, France) (WWW '22). Association for Computing Machinery, New York, NY, USA, 1009–1018.
- [9] Felipe L. Gewers, Gustavo R. Ferreira, Henrique F. De Arruda, Filipi N. Silva, Cesar H. Comin, Diego R. Amancio, and Luciano Da F. Costa. 2021. Principal Component Analysis: A Natural Approach to Data Exploration. ACM Comput. Surv. 54, 4, Article 70 (May 2021), 34 pages.
- [10] Walter R. Gilks and Pascal Wild. 1992. Adaptive Rejection Sampling for Gibbs Sampling. Quality Engineering 37 (1992), 417–420.
- [11] Xavier Glorot and Yoshua Bengio. 2010. Understanding the difficulty of training deep feedforward neural networks. In International Conference on Artificial Intelligence and Statistics.
- [12] Ivan Gutman. 2001. The Energy of a Graph: Old and New Results. In Algebraic Combinatorics and Applications, Anton Betten, Axel Kohnert, Reinhard Laue, and Alfred Wassermann (Eds.). Springer Berlin Heidelberg, Berlin, Heidelberg, 196–211.
- [13] William L. Hamilton, Zhitao Ying, and Jure Leskovec. 2017. Inductive Representation Learning on Large Graphs. In Neural Information Processing Systems.
- [14] Xiangnan He, Kuan Deng, Xiang Wang, Yan Li, Yongdong Zhang, and Meng Wang. 2020. LightGCN: Simplifying and Powering Graph Convolution Network for Recommendation. Proceedings of the 43rd International ACM SIGIR Conference on Research and Development in Information Retrieval (2020).
- [15] Xiangnan He, Lizi Liao, Hanwang Zhang, Liqiang Nie, Xia Hu, and Tat-Seng Chua. 2017. Neural Collaborative Filtering. In Proceedings of the 26th International Conference on World Wide Web (Perth, Australia) (WWW '17). International World Wide Web Conferences Steering Committee, Republic and Canton of Geneva, CHE. 173–182.
- [16] Geoffrey E. Hinton. 2022. The Forward-Forward Algorithm: Some Preliminary Investigations. ArXiv abs/2212.13345 (2022).
- [17] Geoffrey E. Hinton and Richard S. Zemel. 1993. Autoencoders, minimum description length and Helmholtz free energy. In Proceedings of the 7th International Conference on Neural Information Processing Systems (Denver, Colorado) (NIPS'93). Morgan Kaufmann Publishers Inc., San Francisco, CA, USA, 3–10.
- [18] Jonathan Ho, Ajay Jain, and Pieter Abbeel. 2020. Denoising diffusion probabilistic models. In Proceedings of the 34th International Conference on Neural Information Processing Systems (Vancouver, BC, Canada) (NIPS '20). Curran Associates Inc., Red Hook, NY, USA, Article 574, 12 pages.
- [19] Emiel Hoogeboom, Didrik Nielsen, Priyank Jaini, Patrick Forré, and Max Welling. 2021. Argmax flows and multinomial diffusion: learning categorical distributions. In Proceedings of the 35th International Conference on Neural Information Processing Systems (NIPS '21). Curran Associates Inc., Red Hook, NY, USA, Article 953, 12 pages.
- [20] Yu Hou, Jin-Duk Park, and Won-Yong Shin. 2024. Collaborative Filtering Based on Diffusion Models: Unveiling the Potential of High-Order Connectivity. In Proceedings of the 47th International ACM SIGIR Conference on Research and Development in Information Retrieval (Washington DC, USA) (SIGIR '24). Association for Computing Machinery, New York, NY, USA, 1360–1369.
- [21] Tinglin Huang, Yuxiao Dong, Ming Ding, Zhen Yang, Wenzheng Feng, Xinyu Wang, and Jie Tang. 2021. MixGCF: An Improved Training Method for Graph Neural Network-based Recommender Systems. Proceedings of the 27th ACM SIGKDD Conference on Knowledge Discovery & Data Mining (2021).
- [22] Aapo Hyvärinen. 2005. Estimation of Non-Normalized Statistical Models by Score Matching. Journal of Machine Learning Research 6, 24 (2005), 695–709.
- [23] Shuyi Ji, Yifan Feng, Rongrong Ji, Xibin Zhao, Wanwan Tang, and Yue Gao. 2020. Dual Channel Hypergraph Collaborative Filtering. Proceedings of the 26th ACM SIGKDD International Conference on Knowledge Discovery & Data Mining (2020).
- [24] Chanwoo Kim, Jinkyu Sung, Yebonn Han, and Joonseok Lee. 2025. Graph Spectral Filtering with Chebyshev Interpolation for Recommendation. In Proceedings of the 48th International ACM SIGIR Conference on Research and Development in Information Retrieval.
- [25] Diederik Kingma and Jimmy Ba. 2015. Adam: A Method for Stochastic Optimization. In International Conference on Learning Representations (ICLR). San Diega, CA. USA.
- [26] Diederik P. Kingma and Max Welling. 2014. Auto-Encoding Variational Bayes. In 2nd International Conference on Learning Representations, ICLR 2014, Banff, AB, Canada, April 14-16, 2014, Conference Track Proceedings.

- [27] Thomas N. Kipf and Max Welling. 2017. Semi-Supervised Classification with Graph Convolutional Networks. In International Conference on Learning Representations.
- [28] Riwei Lai, L. Chen, Yuhan Zhao, R. Chen, and Qilong Han. 2023. Disentangled Negative Sampling for Collaborative Filtering. Proceedings of the Sixteenth ACM International Conference on Web Search and Data Mining (2023).
- [29] Riwei Lai, Rui Chen, Qilong Han, Chi Zhang, and Li Chen. 2024. Adaptive hardness negative sampling for collaborative filtering. In Proceedings of the Thirty-Eighth AAAI Conference on Artificial Intelligence and Thirty-Sixth Conference on Innovative Applications of Artificial Intelligence and Fourteenth Symposium on Educational Advances in Artificial Intelligence (AAAI'24/IAAI'24/EAAI'24). AAAI Press, Article 961, 8 pages. doi:10.1609/aaai.v38i8.28709
- [30] Jiuqiang Li and Hongjun Wang. 2024. Graph Diffusive Self-Supervised Learning for Social Recommendation. In Proceedings of the 47th International ACM SIGIR Conference on Research and Development in Information Retrieval (Washington DC, USA) (SIGIR '24). Association for Computing Machinery, New York, NY, USA, 2442–2446.
- [31] Qimai Li, Zhichao Han, and Xiao-Ming Wu. 2018. Deeper insights into graph convolutional networks for semi-supervised learning. In Proceedings of the Thirty-Second AAAI Conference on Artificial Intelligence.
- [32] Xiaodong Li, Hengzhu Tang, Jiawei Sheng, Xinghua Zhang, Li Gao, Suqi Cheng, Dawei Yin, and Tingwen Liu. 2025. Exploring Preference-Guided Diffusion Model for Cross-Domain Recommendation. In Proceedings of the 31st ACM SIGKDD Conference on Knowledge Discovery and Data Mining V.1 (Toronto ON, Canada) (KDD '25). Association for Computing Machinery, New York, NY, USA, 719–728.
- [33] Zongwei Li, Lianghao Xia, and Chao Huang. 2024. RecDiff: Diffusion Model for Social Recommendation. In Proceedings of the 33rd ACM International Conference on Information and Knowledge Management (Boise, ID, USA) (CIKM '24). Association for Computing Machinery, New York, NY, USA, 1346–1355.
- [34] Dawen Liang, Rahul G. Krishnan, Matthew D. Hoffman, and Tony Jebara. 2018. Variational Autoencoders for Collaborative Filtering. In Proceedings of the 2018 World Wide Web Conference (Lyon, France) (WWW '18). International World Wide Web Conferences Steering Committee, Republic and Canton of Geneva, CHE, 689–698.
- [35] Sungbin Lim, Eunbi Yoon, Taehyun Byun, Taewon Kang, Seungwoo Kim, Kyung-jae Lee, and Sungjoon Choi. 2023. Score-based generative modeling through stochastic evolution equations in hilbert spaces. In Proceedings of the 37th International Conference on Neural Information Processing Systems (New Orleans, LA, USA) (NIPS '23). Curran Associates Inc., Red Hook, NY, USA, Article 1645, 14 pages.
- [36] Jianghao Lin, Jiaqi Liu, Jiachen Zhu, Yunjia Xi, Chengkai Liu, Yangtian Zhang, Yong Yu, and Weinan Zhang. 2024. A Survey on Diffusion Models for Recommender Systems. ArXiv abs/2409.05033 (2024).
- [37] Jiahao Liu, Dongsheng Li, Hansu Gu, Tun Lu, P. Zhang, Li Shang, and Ning Gu. 2023. Personalized Graph Signal Processing for Collaborative Filtering. Proceedings of the ACM Web Conference 2023 (2023).
- [38] Shuo Liu, An Zhang, Guoqing Hu, Hong Qian, and Tat-Seng Chua. 2025. Preference Diffusion for Recommendation. In The Thirteenth International Conference on Learning Representations.
- [39] Trung-Kien Nguyen and Yuan Fang. 2024. Diffusion-based Negative Sampling on Graphs for Link Prediction. In Proceedings of the ACM Web Conference 2024 (Singapore, Singapore) (WWW '24). Association for Computing Machinery, New York, NY, USA, 948–958.
- [40] Shaowen Peng, Xin Liu, Kazunari Sugiyama, and Tsunenori Mine. 2024. How Powerful is Graph Filtering for Recommendation. In Proceedings of the 30th ACM SIGKDD Conference on Knowledge Discovery and Data Mining (Barcelona, Spain) (KDD '24). Association for Computing Machinery, New York, NY, USA, 2388–2399
- [41] Raksha Ramakrishna, Hoi-To Wai, and Anna Scaglione. 2020. A User Guide to Low-Pass Graph Signal Processing and Its Applications: Tools and Applications. IEEE Signal Processing Magazine 37 (2020), 74–85.
- [42] Steffen Rendle, Christoph Freudenthaler, Zeno Gantner, and Lars Schmidt-Thieme. 2009. BPR: Bayesian Personalized Ranking from Implicit Feedback. ArXiv abs/1205.2618 (2009).
- [43] Danilo Rezende and Shakir Mohamed. 2015. Variational Inference with Normalizing Flows. In Proceedings of the 32nd International Conference on Machine Learning (Proceedings of Machine Learning Research, Vol. 37), Francis Bach and David Blei (Eds.). PMLR, Lille, France, 1530–1538.
- [44] C. E. Shannon. 2001. A mathematical theory of communication. SIGMOBILE Mob. Comput. Commun. Rev. 5, 1 (Jan. 2001), 3–55.
- [45] Jie Shuai, Kun Zhang, Le Wu, Peijie Sun, Richang Hong, Meng Wang, and Yong Li. 2022. A Review-aware Graph Contrastive Learning Framework for Recommendation. Proceedings of the 45th International ACM SIGIR Conference on Research and Development in Information Retrieval (2022).
- [46] David I. Shuman, Sunil K. Narang, Pascal Frossard, Antonio Ortega, and Pierre Vandergheynst. 2012. The emerging field of signal processing on graphs: Extending high-dimensional data analysis to networks and other irregular domains. IEEE Signal Processing Magazine 30 (2012), 83–98.

- [47] Manfred J. Sippl, Maria Ortner, Markus Jaritz, Peter Lackner, and Hannes Flöckner. 1996. Helmholtz free energies of atom pair interactions in proteins. Folding & design 1 4 (1996), 289–98.
- [48] Jascha Sohl-Dickstein, Eric A. Weiss, Niru Maheswaranathan, and Surya Ganguli. 2015. Deep unsupervised learning using nonequilibrium thermodynamics. In Proceedings of the 32nd International Conference on International Conference on Machine Learning - Volume 37 (Lille, France) (ICML'15). JMLR.org, 2256–2265.
- [49] Jianing Sun, Zhaoyue Cheng, Saba Zuberi, Felipe Perez, and Maksims Volkovs. 2021. HGCF: Hyperbolic Graph Convolution Networks for Collaborative Filtering (WWW '21). Association for Computing Machinery, New York, NY, USA, 593–601.
- [50] Sophia Tang, Yinuo Zhang, Alexander Tong, and Pranam Chatterjee. 2025. Gumbel-Softmax Score and Flow Matching for Discrete Biological Sequence Generation. In ICLR 2025 Workshop on AI for Nucleic Acids.
- [51] Yee Whye Teh, Max Welling, Simon Osindero, and Geoffrey E. Hinton. 2003. Energy-based models for sparse overcomplete representations. J. Mach. Learn. Res. 4, null (Dec. 2003), 1235–1260.
- [52] Petar Veličković, Guillem Cucurull, Arantxa Casanova, Adriana Romero, Pietro Liò, and Yoshua Bengio. 2018. Graph Attention Networks. In International Conference on Learning Representations.
- [53] Pascal Vincent. 2011. A Connection Between Score Matching and Denoising Autoencoders. Neural Computation 23, 7 (2011), 1661–1674.
- [54] Joojo Walker, Ting Zhong, Fengli Zhang, Qiang Gao, and Fan Zhou. 2022. Recommendation via Collaborative Diffusion Generative Model. In Knowledge Science, Engineering and Management: 15th International Conference, KSEM 2022, Singapore, August 6–8, 2022, Proceedings, Part III (Singapore, Singapore). Springer-Verlag, Berlin, Heidelberg, 593–605.
- [55] Wenjie Wang, Yiyan Xu, Fuli Feng, Xinyu Lin, Xiangnan He, and Tat-Seng Chua. 2023. Diffusion Recommender Model. In Proceedings of the 46th International ACM SIGIR Conference on Research and Development in Information Retrieval (Taipei, Taiwan) (SIGIR '23). Association for Computing Machinery, New York, NY, USA, 832–841.
- [56] Jiancan Wu, Xiang Wang, Fuli Feng, Xiangnan He, Liang Chen, Jianxun Lian, and Xing Xie. 2020. Self-supervised Graph Learning for Recommendation. Proceedings of the 44th International ACM SIGIR Conference on Research and Development in Information Retrieval (2020).
- [57] Yao Wu, Christopher DuBois, Alice X. Zheng, and Martin Ester. 2016. Collaborative Denoising Auto-Encoders for Top-N Recommender Systems. In Proceedings of the Ninth ACM International Conference on Web Search and Data Mining (San Francisco, California, USA) (WSDM '16). Association for Computing Machinery, New York, NY, USA, 153–162.
- [58] Lianghao Xia, Chao Huang, Yong Xu, Jiashu Zhao, Dawei Yin, and J. Huang. 2022. Hypergraph Contrastive Collaborative Filtering. Proceedings of the 45th International ACM SIGIR Conference on Research and Development in Information Retrieval (2022).
- [59] Rui Xia, Yanhua Cheng, Yongxiang Tang, Xiaocheng Liu, Xialong Liu, Lisong Wang, and Peng Jiang. 2025. S-Diff: An Anisotropic Diffusion Model for Collaborative Filtering in Spectral Domain. In Proceedings of the Eighteenth ACM International Conference on Web Search and Data Mining (Hannover, Germany) (WSDM '25). Association for Computing Machinery, New York, NY, USA, 70–78.
- [60] Tao Yang, Jian Chang, Bo Ren, Ming C. Lin, Jian Jun Zhang, and Shi-Min Hu. 2015. Fast multiple-fluid simulation using Helmholtz free energy. ACM Trans. Graph. 34, 6, Article 201 (Nov. 2015), 11 pages.
- [61] Zhen Yang, Ming Ding, Tinglin Huang, Yukuo Cen, Junshuai Song, Bin Xu, Yuxiao Dong, and Jie Tang. 2024. Does Negative Sampling Matter? A Review with Insights into its Theory and Applications. IEEE transactions on pattern analysis and machine intelligence PP (2024).
- [62] Z. Yang, Ming Ding, Chang Zhou, Hongxia Yang, Jingren Zhou, and Jie Tang. 2020. Understanding Negative Sampling in Graph Representation Learning. Proceedings of the 26th ACM SIGKDD International Conference on Knowledge Discovery & Data Mining (2020).
- [63] Zhengyi Yang, Jiancan Wu, Zhicai Wang, Xiang Wang, Yancheng Yuan, and Xiangnan He. 2023. Generate What You Prefer: Reshaping Sequential Recommendation via Guided Diffusion. In Thirty-seventh Conference on Neural Information Processing Systems.
- [64] Rex Ying, Ruining He, Kaifeng Chen, Pong Eksombatchai, William L. Hamilton, and Jure Leskovec. 2018. Graph Convolutional Neural Networks for Web-Scale Recommender Systems. Proceedings of the 24th ACM SIGKDD International Conference on Knowledge Discovery & Data Mining (2018).
- [65] Junliang Yu, Xin Xia, Tong Chen, Lizhen Cui, Nguyen Quoc Viet Hung, and Hongzhi Yin. 2023. XSimGCL: Towards Extremely Simple Graph Contrastive Learning for Recommendation. IEEE Trans. on Knowl. and Data Eng. (2023).
- [66] Meng Yuan, Yutian Xiao, Wei Chen, Chou Zhao, Deqing Wang, and Fuzhen Zhuang. 2025. Hyperbolic Diffusion Recommender Model. In Proceedings of the ACM on Web Conference 2025 (Sydney NSW, Australia) (WWW '25). Association for Computing Machinery, New York, NY, USA, 1992–2006.
- [67] Yin Zhang, Derek Zhiyuan Cheng, Tiansheng Yao, Xinyang Yi, Lichan Hong, and Ed H. Chi. 2020. A Model of Two Tales: Dual Transfer Learning Framework for Improved Long-tail Item Recommendation. Proceedings of the Web Conference

Helmholtz Free Energy $H \uparrow \equiv U \uparrow -tS \downarrow$								
Acronym	Thermodynamics	Informatics	Target					
H	Free energy to be obtained for useful work	Generalized useful pattern for accurate prediction	Performance					
\mathbf{U}	Internal energy of a thermodynamic system	Information quantity of the training data	Reconstruction					
S	Entropy causing spontaneous processes	Magnitude of uncertainty in information	Refinement					
t	Given temperature of the system	Given priorities of two metrics in model	Coefficient					

Table 5: Comparison between thermodynamics and informatics in terms of Helmholtz free energy.

2021 (2020).

- [68] Chu Zhao, Enneng Yang, Yuliang Liang, Pengxiang Lan, Yuting Liu, Jianzhe Zhao, Guibing Guo, and Xingwei Wang. 2025. Graph Representation Learning via Causal Diffusion for Out-of-Distribution Recommendation. In Proceedings of the ACM on Web Conference 2025 (Sydney NSW, Australia) (WWW '25). Association for Computing Machinery, New York, NY, USA, 334–346.
- [69] Chu Zhao, Enneng Yang, Yuliang Liang, Jianzhe Zhao, Guibing Guo, and Xingwei Wang. 2025. Symmetric Graph Contrastive Learning against Noisy Views for Recommendation. ACM Trans. Inf. Syst. 43, 3, Article 80 (May 2025), 28 pages.
- [70] Jujia Zhao, Wang Wenjie, Yiyan Xu, Teng Sun, Fuli Feng, and Tat-Seng Chua. 2024. Denoising Diffusion Recommender Model. In Proceedings of the 47th International ACM SIGIR Conference on Research and Development in Information Retrieval (Washington DC, USA) (SIGIR '24). Association for Computing Machinery, New York, NY, USA, 1370–1379.
- [71] Yunqin Zhu, Chao Wang, Qi Zhang, and Hui Xiong. 2024. Graph Signal Diffusion Model for Collaborative Filtering. In Proceedings of the 47th International ACM SIGIR Conference on Research and Development in Information Retrieval (Washington DC, USA) (SIGIR '24). Association for Computing Machinery, New York, NY, USA, 1380–1390.
- [72] Royce K. P. Zia, Edward F. Redish, and Susan R. McKay. 2008. Making sense of the Legendre transform. American Journal of Physics 77 (2008), 614–622.

A Discussion on Helmholtz Free Energy

Helmholtz free energy is originally defined via a Legendre transformation [72] on the fundamental thermodynamic relation. Starting from the internal energy U, a function of entropy S and volume V, the transformation replaces energy and entropy with their conjugate variable, temperature $\mathbf{t} = (\partial U/\partial S)|_V$, as the independent variable for volume-agnostic processes. Over the years, it has been adopted across a variety of domains, such as chemistry [6], biology [47], and computer graphics [60]. Hinton and Zemel [17] first introduced this concept into machine learning. They illustrated that the objective function minimized by autoencoders is mathematically equivalent to optimizing a bound on the description length under the Minimum Description Length (MDL) principle, minimizing the Helmholtz free energy statistically in the meanwhile. Thus, the MDL goal and the variational approximation of the Helmholtz free energy manifest as a trade-off optimized by autoencoders, where the reconstruction accuracy term is balanced by a constraint on the capacity of the latent representation. In spite of previous work, our work mainly focuses on diffusion- and graph-based recommendation tasks, inspired by a series of our designated experiments. For better understanding, we summarize the similarities in Helmholtz free energy between thermodynamics and informatics (cf. Table 5).

B Proof for Equivalence of Entropy and BPR

As *entropy*-based training objectives, Binary Cross Entropy (BCE) explicitly optimizes the models by decreasing the *entropy*, while the mechanism of BPR is subtle. According to Observation 2 (cf. Figure 2 & 3), we experimentally prove the equivalence between *entropy* and BPR. Here, we derive it theoretically:

THEOREM B.1. BPR loss is equivalent to the entropy, that is, model optimization by BPR loss will reduce the entropy in the meantime.

PROOF. By definition, we have:

$$S(u) = -\hat{\mathbf{r}}_u \log \hat{\mathbf{r}}_u^{\mathsf{T}},\tag{18}$$

where $\hat{\mathbf{r}}_u = \exp(\tilde{\mathbf{r}}_u)/\|\exp(\tilde{\mathbf{r}}_u)\|_1 = \exp(\tilde{\mathbf{r}}_u)/(n \cdot \mathbb{E}[\exp(\tilde{\mathbf{r}}_{u,*})])$. Since the entropy computation is based on probability vectors $\hat{\mathbf{r}}_u$, we reformulate the BPR loss in the form of vectors by $\tilde{\mathbf{r}}_u$ as well:

$$\mathcal{L}_{BPR}(u) = \sum_{i \in N(u), j \notin N(u)} -\log \sigma(\tilde{r}_{u,i} - \tilde{r}_{u,j}),$$

$$\equiv \|-\log \sigma(\tilde{r}_u - \mathbb{E}[\tilde{r}_{u,*}])\|_{1},$$
(19)

where we substitute the score of negative items with the expectation of score among all items $\mathbb{E}[\tilde{r}_{u,*}]$ for user u. The rationales for it are: (1) item sets usually adhere to the long-tail distribution during to the high sparity, where most items are non-interactive, i.e., $\mathbb{E}[\tilde{r}_{u,-}] \approx \mathbb{E}[\tilde{r}_{u,*}]$; and (2) the score of interactive items is always non-negative during training, i.e., $\tilde{r}_{u,+} \geq 0$, making the cost for mistaking the interactive items for negative samples bounded. Hence, this substitution is harmless to the model optimization.

When BPR loss converges:

$$\frac{\partial \mathcal{L}_{BPR}}{\partial \tilde{r}_{u}} = -\frac{1}{\sigma(\cdot)} \cdot \frac{\partial \sigma(\cdot)}{\partial \tilde{r}_{u}} = -\frac{1}{\sigma(\cdot)} \cdot (1 - \sigma(\cdot)) = -\frac{1}{\sigma(\cdot)} + 1 = 0, (20)$$

$$\sigma(\tilde{r}_{u} - \mathbb{E}[\tilde{r}_{u,*}]) = 1$$

$$\exp(-(\tilde{r}_{u} - \mathbb{E}[\tilde{r}_{u,*}])) = 0$$

$$\exp(-\tilde{r}_{u}) \cdot \exp(\mathbb{E}[\tilde{r}_{u,*}]) = 0.$$

According to the Jensen's Inequality, we have:

$$\exp(\mathbb{E}[\tilde{r}_{u,*}]) \le \mathbb{E}[\exp(\tilde{r}_{u,*})], \tag{22}$$

since $\exp(\cdot)$ is a convex function. Hence, we decompose the BPR convergence condition into two sub-conditions: ① Equality holds for $\tilde{\jmath}ensen$'s Inequality, i.e, $\tilde{r}_{u,1} = \cdots = \tilde{r}_{u,n}$, and ② gradient of the updated BPR loss becomes 0, i.e., $\exp(-\tilde{r}_u) \cdot \mathbb{E}[\exp(\tilde{r}_{u,*})] = 0$. Thus, the definition of entropy can be updated as follows:

$$S(u) = -\frac{\exp(\tilde{r}_{u})}{n \cdot \mathbb{E}[\exp(\tilde{r}_{u,*})]} \left(\log \frac{\exp(\tilde{r}_{u})}{n \cdot \mathbb{E}[\exp(\tilde{r}_{u,*})]}\right)^{\top}$$

$$= \frac{1}{n} \cdot \underbrace{\frac{\exp(\tilde{r}_{u})}{\mathbb{E}[\exp(\tilde{r}_{u,*})]}}_{\text{one for } 2} \left(\log \left(\underbrace{\frac{\mathbb{E}[\exp(\tilde{r}_{u,*})]}{\exp(\tilde{r}_{u})}}\right) + \underbrace{\log n}_{\text{const.}}\right)^{\top} \to -\infty, \quad (23)$$

where $\lim_{x\to 0} \log x = -\infty$.

REMARK. Regarding a stable training process, the first term (cf. Eq. (23)) cannot satisfy condition ② as it will inevitably confront a gradient explosion when 0 serves as the denominator of fractions. Besides, to hold both conditions, the condition ② has to be assigned to the second term as a necessity. Although the co-constraints of both conditions preclude a closed-form solution, the BPR loss exhibits monotonic optimization behavior alongside decreasing entropy in this configuration.

C Proof for Higher Entropy on Multi-Layer Message-Passing

To explore the higher *entropy* achieved via multi-layer message-passing, we first rigorously characterize its higher smoothness compared with single-layer message-passing. It is worth noting that the message-passing mechanism we are about to prove is a linear process as defined by LightGCN [14].

PROPOSITION C.1 ([41]). Given a graph G with its corresponding normalized Laplacian matrix \bar{L} , the eigenvalues of \bar{L} are $\bar{\lambda}_i \in [0,2]$, such that the eigenvalues of the symmetric normalized adjacency matrix $\bar{A} = \begin{bmatrix} 0 & \bar{R} \\ \bar{L} & \bar{L} \end{bmatrix} \in \mathbb{R}^{(m+n)\times(m+n)}$ after eigendecomposition are:

$$\begin{aligned} & \textit{matrix} \ \bar{\pmb{A}} = \begin{bmatrix} \mathbb{0} & \bar{\pmb{R}} \\ \bar{\pmb{R}}^\top & \mathbb{0} \end{bmatrix} \in \mathbb{R}^{(m+n)\times(m+n)} \ \textit{after eigendecomposition are:} \\ & -1 \leq (1-\bar{\lambda}_1) \leq \cdots \leq (1-\bar{\lambda}_{m+n}) \leq 1. \end{aligned}$$

Proposition C.2. When the over-smoothing phenomenon in BP-based graph learning occurs, all low and middle frequencies of signals, except for the lowest and highest ones, will be removed, i.e., $\forall \bar{\lambda}_i \in (0,2), (1-\bar{\lambda}_i)^{\infty} \to 0$.

Theorem C.3. Single-layer message-passing learns NO less different frequencies of signals than multi-layer message-passing, i.e., $(\forall \bar{\lambda}_i \in [0,1]) \land (\forall \alpha_k > 0) \land (\forall K \in \mathbb{Z}^+), (1-\bar{\lambda}_i) \geq [\sum_{k=1}^K \alpha_k (1-\bar{\lambda}_i)^k]/\sum_{k=1}^K \alpha_k$, where α_k denotes the attention score of layer k.

PROOF. We prove it by mathematical induction. First, let $\mathcal{F}_G'(K) = [\sum_{k=1}^K \alpha_k (1-\bar{\lambda}_i)^k]/\sum_{k=1}^K \alpha_k, \mathcal{F}_G = 1-\tilde{\lambda}_i$. When K=1, $\mathcal{F}_G'(1)=(1-\bar{\lambda}_i)$. Hence, $\mathcal{F}_G'(1)\leq \mathcal{F}_G$ is true. Assume $\mathcal{F}_G'(K)\leq \mathcal{F}_G$ for all K>1. Then, we can prove that:

$$\mathcal{F}'_{G}(K+1) = \left[\sum_{k=1}^{K} \alpha_{k} (1 - \bar{\lambda}_{i})^{k} + \alpha_{K+1} (1 - \bar{\lambda}_{i})^{K+1}\right] / \left[\sum_{k=1}^{K} \alpha_{k} + \alpha_{K+1}\right],$$

$$\mathcal{F}_{G} - \mathcal{F}'_{G}(K+1) = \left[\sum_{k=1}^{K} \alpha_{k} (1 - \bar{\lambda}_{i}) - \sum_{k=1}^{K} \alpha_{k} (1 - \bar{\lambda}_{i})^{k}\right]$$

$$+ \left[\alpha_{K+1} (1 - \bar{\lambda}_{i}) - \alpha_{K+1} (1 - \bar{\lambda}_{i})^{K+1}\right] \ge 0.$$
(25)

With assumptions, the first term (cf. Eq. (24)) and the second term (cf. Eq. (25)) are greater than or equal to 0 under the given Proposition C.2. Hence, $\mathcal{F}_G \geq \mathcal{F}_G'(K)$ for all $\bar{\lambda}_i \in [0,1]$ when $K \in \mathbb{Z}^+$ and $\alpha_k > 0$. Similar conclusions can be drawn for high-frequency signals, i.e., $\bar{\lambda}_i \in [1,2]$, since we only focus the magnitude ($|\mathcal{F}_G| \geq |\mathcal{F}_G'(K)|$) rather than the direction (similar or dissimilar).

Remark. We omit the input embedding since we empirically find significant performance gains after skipping it in practice. Due to the absence of an associated filter, the input embedding leads to unstable training. Nonetheless, the proof with input embedding is still derivable, where both methods shall share the same scores α_0 and α_1 .

PROPOSITION C.4. Given the graph quadratic form $S(\mathbf{x}) = \mathbf{x}^{\top} \bar{\mathbf{L}} \mathbf{x}$ where $\bar{\mathbf{L}}$ is the Laplacian matrix, a lower value of $S(\mathbf{x})$ indicates a smoother signal \mathbf{x} [46]. Thus, $\nabla S(\mathbf{x} \mid \mathbf{x}') = S(\mathbf{x})S^{-1}(\mathbf{x}')$ represents the difference of smoothness between \mathbf{x} and $\mathbf{x}' : \nabla S(\mathbf{x} \mid \mathbf{x}') > 1$ states signal \mathbf{x} is sharper than signal \mathbf{x}' , and vice versa.

Theorem C.5. Single-layer message-passing fosters a NO smoother reconstructed joint scores matrix $\tilde{\mathbf{A}}_S$ than $\tilde{\mathbf{A}}_M$ that is retrieved from in multi-layer message-passing, i.e., $\nabla S(\tilde{\mathbf{A}}_S \mid \tilde{\mathbf{A}}_M) \geq \mathbf{I}$.

PROOF. First, since the logarithm and sigmoid are element-wise and monotone-increasing functions, we have the definition of raw recommendation predictions:

$$\tilde{a}_{u,i} = \log \sigma(\tilde{a}_{u,i}) \propto \boldsymbol{e}_{u} \boldsymbol{e}_{i}^{\top}$$

$$\iff \tilde{A} = \log \sigma(\boldsymbol{E}_{final} \boldsymbol{E}_{final}^{\top}) \propto \boldsymbol{E}_{final} \boldsymbol{E}_{final}^{\top}, \tag{26}$$

where $\sigma(\cdot)$ denotes the sigmoid function. Hence, the pivotal point of proof lies in the similarity matrix derived from the self-multiplication

of the final embedding
$$E_{final} = \begin{bmatrix} E_{\mathcal{U}} \\ E_{\mathcal{I}} \end{bmatrix} \in \mathbb{R}^{(m+n) \times d}$$
.

Next, let $\bar{A}' = [\sum_{k=1}^K \alpha_k \bar{A}^k]/\sum_{k=1}^K \alpha_k$ as the equivalent adjacency matrix for multi-layer message-passing. Also, let $X = E_{final}E_{final}^{\mathsf{T}} = \bar{A}E_0E_0^{\mathsf{T}}\bar{A}^{\mathsf{T}}$ and $X' = E_{final}'E_{final}' = \bar{A}'E_0E_0^{\mathsf{T}}\bar{A}'^{\mathsf{T}}$ denote the similarity matrices from single-layer and multi-layer message-passing, respectively. Hence, we have:

$$XX'^{-1} = \bar{A}E_{0}E_{0}^{\top}\bar{A}^{\top}(\bar{A}'E_{0}E_{0}^{\top}\bar{A}'^{\top})^{-1}$$

$$\geq \bar{A}E_{0}E_{0}^{\top}I(\bar{A}'E_{0}E_{0}^{\top})^{-1} = \bar{A}(\bar{A'}^{\top})^{-1} \geq I,$$
(27)

where $\bar{A}\bar{A'}^{\top} = \bar{U}(I-\bar{\Lambda})(I-\bar{\Lambda}')^{-1}\bar{U}^{\top} \geq \bar{U}(I-\bar{\Lambda}')(I-\bar{\Lambda}')^{-1}\bar{U}^{\top} = I$ since $(I-\bar{\Lambda}) \geq (I-\bar{\Lambda}')$ by Theorem C.3 and \bar{U} is the orthogonal matrix, i.e., $\bar{U}^{\top} = \bar{U}^{-1}$.

Then, we delve into the difference of smoothness between \boldsymbol{X} and \boldsymbol{X}' by Eq. (27), we have:

$$\nabla \mathcal{S}(\tilde{A}_{S} \mid \tilde{A}_{M}) = \boldsymbol{X}^{\top} \bar{L} \boldsymbol{X} (\boldsymbol{X}'^{\top} \bar{L} \boldsymbol{X}')^{-1}$$

$$\geq \boldsymbol{X}^{\top} \bar{L} \boldsymbol{I} (\boldsymbol{X}'^{\top} \bar{L})^{-1} = \boldsymbol{X}^{\top} (\boldsymbol{X}'^{\top})^{-1} \geq \boldsymbol{I}.$$
(28)

By Eq. (26) and Eq. (28), we can see that the whole scores matrix in single-layer message-passing is NO smoother than those in multi-layer message-passing. With the increment of layers, the scores for all items tend to be similar and move towards a uniform distribution. Consequently, *entropy* increases towards the maximum, potentially resulting in the over-smoothing issue [31].

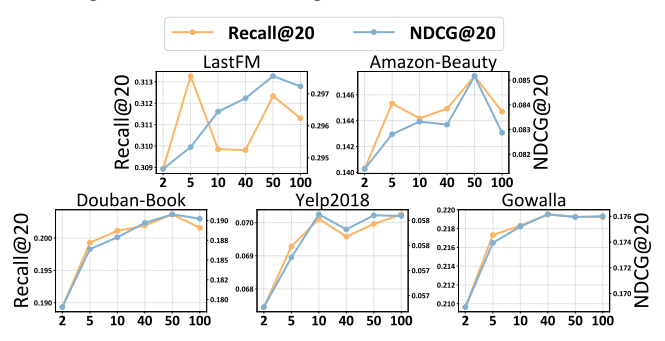


Figure 8: Influence of the number of diffusion timesteps T.

D Supplementary Experiments

Hyperparameter Sensitivity Analysis for diffusion timestep

T. We analyze the sensitivity of the key hyperparameter in diffusion models: diffusion timestep T. This parameter bounds the maximum step for the forward and reverse processes. We vary T in the range $\{2, 5, 10, 40, 50 100\}$ as designed in [55]. According to the results (cf. Figure 8), TV-Diff consistently reaches a peak when T = 50 for both small datasets and large datasets. This phenomenon suggests that a large diffusion timestep helps better simulate the denoising

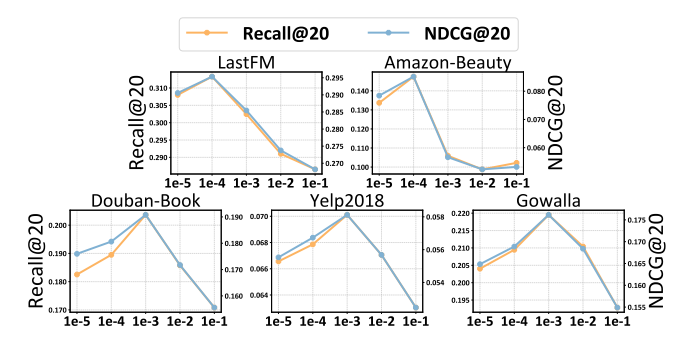


Figure 9: Influence of the noise scale s.

process, facilitating the underlying score-matching mechanism to capture the comprehensive distributions.

Hyperparameter Sensitivity Analysis for noise scale s. We also analyze the sensitivity of another key hyperparameter in diffusion models: noise scale s. This parameter controls the magnitude of the added noise in different timesteps. We vary s in the range {1e-5, 1e-4, 1e-3, 1e-2, 1e-1} as designed in [55]. According to the results (cf. Figure 9), TV-Diff reaches a peak when s = 1e - 4 and s = 1e - 3 for small datasets and large datasets, respectively. This phenomenon suggests that a small noise scale helps diffusion models to learn the nuanced distribution for small datasets, while large datasets exhibit robustness to a large noise scale.

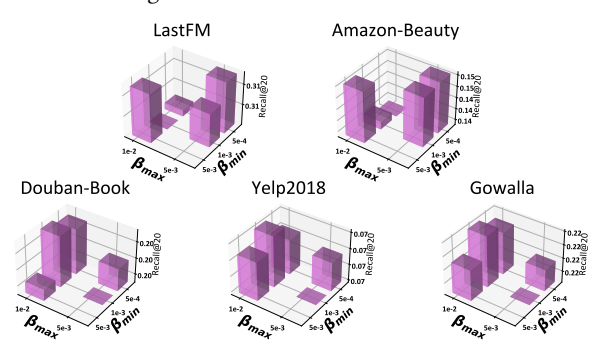


Figure 10: Influence of the upper and lower bound of noise.

Hyperparameter Sensitivity Analysis for the upper & low bound of noise. We finally analyze the sensitivity of the last key hyperparameters in diffusion models: the upper and lower bounds of the noise. These parameters constrain the maximum and minimum noise among the whole processes. We vary them in the range of the $(\beta_{min}, \beta_{max})$ pairs {(5e-4, 5e-3), (5e-4, 1e-3), (1e-3, 5e-3), (1e-3, 1e-2)} as designed in [55]. According to the results (cf. Figure 10), TV-Diff reaches a peak when the pair $(\beta_{min}, \beta_{max}) = (5e-4, 5e-3)$ and $(\beta_{min}, \beta_{max}) = (1e-3, 1e-2)$ for small datasets and large datasets, respectively. This phenomenon suggests that a small difference between the upper and lower bounds helps diffusion models to maintain the consistency of learned distribution for training stability on small datasets, while a large difference provides a variety of mutual information on extreme noise to explore the credible denoising patterns on large datasets.

Impact of Topological Information. We evaluate how incorporating topological information (i.e., symmetric normalization, left normalization, LinkProp [8]) affects the anisotropic denoiser. According to the results 11, the symmetric normalized bipartite

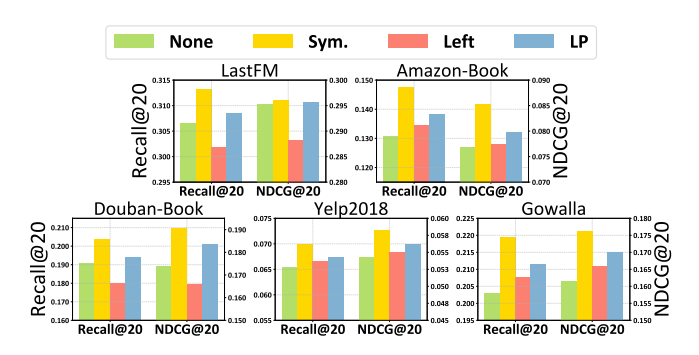


Figure 11: Influence of topological information.

matrix consistently outperforms others, signifying its concise and accurate encoding of anisotropic user and item degree signals. In contrast, the left-normalized matrix fails to involve the item degree information, and the smoothed graph matrix of LinkProp attenuates the anisotropic signals, both resulting in model deterioration.

E Algorithms

Algorithm 1 The training process with TV-Diff

Input: binary interaction X_0 , symmetric normalized \bar{A} , entropy-based training objective \mathcal{L}_S , temperature t, negative factor γ , diffusion-based hyperparameter $(T, s, \beta_{min}, \beta_{max})$.

Output: overall learnable parameters θ

```
1: while not convergent do
          for each batch of users u do
 2:
               Sample t \sim Uniform(1, T);
 3:
               Computer X_t[u] \leftarrow \text{Eq. (1)};
 4:
 5:
               Reconstruct the X_0[u] with \bar{A} \leftarrow \text{Eq. (13), (14)}; \triangleright \text{View II}
 6:
               Sample negative items j \leftarrow \text{Eq. (16), (17)};
                                                                                  ▶ View III
               Compute \mathcal{L}_H by involving \mathcal{L}_S \leftarrow \text{Eq. (9)};
 7:
                                                                                    ▶ View I
               Update by descending gradients \nabla_{\theta} \mathcal{L}_{H};
 8:
          end for
     end while
11: return \theta
```

Algorithm 2 The inference process with TV-Diff

Input: binary interaction X_0 , symmetric normalized \bar{A} , diffusion-based hyperparameter $(T, s, \beta_{min}, \beta_{max})$, optimized parameters θ

Output: reconstructed interaction prediction \tilde{X}_0

```
1: if s > 0 then
2: Sample noise from \mathcal{N}(0, I);
3: end if
4: Computer X_T with noise (if existing) \leftarrow Eq. (1);
5: for each timestep t in [T, \ldots, 1] do
6: Compute \tilde{X}_{t-1} by q(\tilde{X}_{t-1}|\tilde{X}_t, X_0) \leftarrow Eq. (13),(14);
7: end for
8: return \tilde{X}_0
```